Socio-hydrologic data assimilation: Analyzing human-flood interactions by model-data integration

Yohei Sawada[1], Risa Hanazaki[2]

[1] Institute of Engineering Innovation, School of Engineering, the University of Tokyo, Tokyo, Japan

[2] Institute of Industrial Science, the University of Tokyo, Tokyo, Japan

Corresponding author: Y. Sawada, Institute of Engineering Innovation, the University of Tokyo, Tokyo, Japan, 2-11-6, Yayoi, Bunkyo-ku, Tokyo, Japan, yohei.sawada@sogo.t.u-tokyo.ac.jp

Abstract

In socio-hydrology, human-water interactions are simulated by mathematical models. Although the integration of these socio-hydrologic models and observation data is necessary to improve the understanding of the human-water interactions, the methodological development of the model-data integration in socio-hydrology is in its infancy. Here we propose to apply sequential data assimilation, which has been widely used in geoscience, to a socio-hydrological model. We developed particle filtering for a widely adopted flood risk model and performed an idealized observation system simulation experiment and a real-data experiment to demonstrate the potential of the sequential data assimilation in socio-hydrology. In these experiments, the flood risk model's parameters, the input forcing data, and empirical social data were assumed to be somewhat imperfect. We tested if data assimilation can contribute to accurately reconstructing the historical human-flood interactions by integrating these imperfect models and imperfect and sparsely distributed data. Our results highlight that it is important to sequentially constrain both state variables and parameters when the input forcing is uncertain. Our proposed method can accurately estimate the model's unknown parameters even if the true model parameter temporally varies. The small amount of empirical data can significantly improve the simulation skill of the flood risk model.

Therefore, sequential data assimilation is useful to reconstruct historical socio-hydrological processes by the synergistic effect of models and data.

1. Introduction

Socio-hydrology is an emerging research field in which two-way feedbacks between social and water systems are investigated (Sivapalan et al. 2012, 2014). Understanding complex socio-hydrologic phenomena contributes to solving water crises around the world. Socio-hydrology has been recognized as an important scientific grand challenge to meet United Nations' Sustainable Development Goals (Di Baldassarre et al. 2019).

The most popular approach in socio-hydrology is to develop dynamic models which compute non-linear interactions between human and water. For instance, Di Baldassarre et al. (2013) developed a simplified model, which described human-flood interactions, to understand the levee effect in which high levees generate a false sense of security and induce social vulnerabilities to severe floods (see also Viglione et al. 2014; Ciullo et al. 2017). Van Emmerik et al. (2014) developed a stylized model, which described two-way feedbacks between environment and economic activities, to understand the historical competition for water between agricultural development and environment health in Australia (see also Roobavannan et al. 2017). Pande and Savenije (2016) modeled economic activities of smallholder farmers to analyze the agrarian crisis in Marathwada, India. While socio-hydrologic models described above assumed the existence of a single lumped decision maker, Yu et al. (2017) incorporated a collective action into their model and analyzed the dynamics of community-managed flood protection systems in coastal Bangladesh. Please refer to Di Baldassarre et al. (2019) for the comprehensive review of socio-hydrologic modeling.

In addition to these modeling approaches, both qualitative and quantitative data related to socio-hydrologic processes are important to understand human-water interactions. For instance, Mostert (2018) revealed historical changes in river management from water resources development to protection and restoration by analyzing qualitative data. Dang and Konar (2018) applied econometric methods to analyze quantitative data in both human and water domains and quantified the causal relationship between trade openness and water use. Kreibich et al. (2017) performed the detailed case study analysis on paired floods, consecutive flood events which occurred in the same region with the second flood causing significantly lower damage. They found that the reduction of vulnerability played a key role for successful adaptation to the second floods.

Although it is expected that the integration of model and data contributes to accurately understanding the socio-hydrologic processes (Mount et al. 2016), the methodological development of the model-data integration in socio-hydrology is in its infancy. Generally, mathematical models can provide spatiotemporally continuous state variables and quantitative scenarios for future socio-hydrologic developments. In addition, mathematical models can quantitatively provide possible scenarios unrealized in the real-world, which gives the insight to targeted processes (e.g., Viglione et al. 2014). The major limitation of socio-hydrological models is that they are often inaccurate due to the uncertainty in their input forcing, parameters, and descriptions of the processes. On the other hand, hydrologic and social data are often more reliable than numerical models and can provide more complete understanding of the socio-hydrological processes (e.g., Mostert 2018), although data also have uncertainties. However, in many cases, relevant data in socio-hydrology are sparsely distributed so that it is difficult to completely reconstruct the historical socio-hydrologic processes from data. The other limitation of the data-driven approach is that the quantification of the causal relationship cannot be easily done only by empirical data (e.g., Dang and Konar 2018). Considering this advantages and disadvantages of model and data, previous studies used social statistics to calibrate and validate their socio-hydrologic models (e.g., Barendrecht et al. 2019; Roobavannan et al. 2017; Ciullo et al. 2017; van Emmerik et al. 2014; Gonzales and Ajami 2017).

In geosciences, sequential data assimilation has been widely used for the model-data integration. Data assimilation sequentially adjusts the predicted state variables and parameters of dynamic models by integrating observation data into models based on Bayes' theorem. Data assimilation has been widely applied to numerical weather prediction (e.g., Miyoshi and Yamane 2007; Bauer et al. 2015; Poterjoy et al. 2019; Sawada et al. 2019), atmospheric reanalysis (e.g., Kobayashi et al. 2015; Hersbach et al. 2019), and hydrology and land surface modeling (e.g., Moradkhani et al. 2005; Sawada et al. 2015; Rasmussen et al. 2015; Lievens et al. 2017). Applicability of the data assimilation approach to the socio-hydrologic models has yet to be investigated.

In this study, we aim to develop the methodology of sequential data assimilation for the flood risk model proposed by Di Baldassarre et al. (2013). From a series of idealized experiments and a real-data experiment in the city of Rome, we demonstrate the potential of data assimilation to accurately reconstruct the historical human-flood interactions. We focus on the case in which the socio-hydrologic model's parameters, input forcing data, and social data are somewhat inaccurate.

2. Method

2.1. Model

In this study, we used a socio-hydrologic flood risk model proposed by Di Baldassarre et al. (2013). This model conceptualizes human-flood interactions by the set of simple equations which describe the states of flood, economy, technology, politics, and society. Based on this original model of Di Baldassarre et al. (2013), many similar flood risk models have been proposed, validated, and applied (e.g., Viglione et al. 2014; Ciullo et al. 2017; Barendrecht et al. 2019). Here we briefly describe this model. Please refer to Di Baldassarre et al. (2013) for the complete description of this model.

The governing equations of the flood risk model are shown below:

$$F = \begin{cases} 1 - \exp\left(-\frac{W+\xi_H H}{\alpha_H D}\right) & if\ W + \xi_H H > H \\ 0 & if\ W + \xi_H H \leq H \end{cases} \qquad (1)$$

$$R = \begin{cases} \varepsilon_T (W + \xi_H H - H) & if\ (F > 0)\ and\ \left(FG > \gamma_E R\sqrt{G}\right)\ and\ (G - FG > \gamma_E R\sqrt{G}) \\ 0 & otherwise \end{cases}$$

(2)

$$S = \begin{cases} \alpha_S F & if\ (R > 0) \\ F & if\ (R = 0) \end{cases} \qquad (3)$$

$$\frac{dG}{dt} = \rho_E \left(1 - \frac{D}{\lambda_E}\right) G - \Delta(\Upsilon(t))(FG + \gamma_E R\sqrt{G}) \qquad (4)$$

$$\frac{dD}{dt} = (M - \frac{D}{\lambda_P})\frac{\varphi_P}{\sqrt{G}} \tag{5}$$

$$\frac{dH}{dt} = \Delta\big(\Upsilon(t)\big)R - \kappa_T H \tag{6}$$

$$\frac{dM}{dt} = \Delta\big(\Upsilon(t)\big)S - \mu_S M \tag{7}$$

This model has four state variables: G, D, H, and M. G(t) [L^2] is the size of the human settlement; D(t) [L] is the distance of the center of mass of the human settlement from the river; H(t) [L] is the flood protection level (or levee height); M(t) [.] is the social awareness of the flood risk. The timestep was set to annual.

Equation (1) calculates the intensity of flooding events F(t) [.] from the high water level W(t) [L], the height of the levee H(t) [L], and the distance of the human settlement from the river D(t) [L]. Equation (2) calculates R(t) [L], the amount by which the levees are raised responding to the flood event. There are three required conditions under which people decide to raise the levee. First, the flood event occurs. Second, the damage of flood (FG) should be larger than the cost of raising levee. Third, the cost of raising levee should be lower than the wealth remaining after the flooding. Equation (3) shows the magnitude of the psychological shock by the flood event S(t) [.]. If the levee is raised, the psychological shock is assumed to be mitigated. Equation (4) explains the dynamics of

G(t), the size of the human settlement or the wealth of the community. Following the notation of Di Baldassarre et al. (2013), $\Delta(\Upsilon(t)) = 1$ with integral only when time t passes the time of the flooding event (F>0), otherwise, $\Delta(\Upsilon(t)) = 0$. The term $FG + \gamma_E R\sqrt{G}$ (total cost of flood damage and construction of levees) appears only if flood occurs. Equation (5) shows the dynamics of the distance of the center of mass of the human settlement from the river D(t). When the social awareness of the flood risk is high, people tend to live far from the river. Equation (6) computes the dynamics of the flood protection level H(t) and equation (7) shows the dynamics of the social awareness of the flood risk M(t). The explanation of parameters can be found in Table 1.

2.2. Data Assimilation

In this study, we used Sampling Importance Resampling Particle Filtering (SIRPF) as the method of data assimilation. SIRPF has been widely used in hydrologic data assimilation (e.g., Moradkhani et al. 2005; Qin et al. 2009; Sawada et al. 2015). Compared with the other data assimilation algorithms such as ensemble Kalman filter, SIRPF is robust against model nonlinearity and associated non-Gaussian error distribution. The disadvantage of SIRPF is that the infeasible computational resources are required if the numerical model is computationally expensive, which is not the case in the flood risk model.

The flood risk model can be formulated as a discrete state-space dynamic system:

$$\boldsymbol{x}(t+1) = f\big(\boldsymbol{x}(t), \boldsymbol{\theta}, \boldsymbol{u}(t)\big) + \boldsymbol{q}(t) \qquad (8)$$

where $\boldsymbol{x}(t)$ is the state variables (i.e. G, D, H, and M), $\boldsymbol{\theta}$ is the model parameters, $\boldsymbol{u}(t)$ is the external forcing (i.e., the high water level), and $\boldsymbol{q}(t)$ is the noise process which represents the model error. In data assimilation, it is useful to formulate an observation process as follows:

$$\boldsymbol{y}^f(t) = h\big(\boldsymbol{x}(t)\big) + \boldsymbol{r}(t) \qquad (9)$$

where $\boldsymbol{y}^f(t)$ is the simulated observation, h is the observation operator which maps the model's state variables into the observable variables, and $\boldsymbol{r}(t)$ is the noise process which represents the observation error.

The SIRPF is a Monte Carlo approximation of Bayesian update of the state variables and parameters:

$$p(\boldsymbol{x}(t), \boldsymbol{\theta} | \boldsymbol{y}^o(1{:}\,t)) \propto p(\boldsymbol{y}^o(t) | \boldsymbol{x}(t), \boldsymbol{\theta}) p(\boldsymbol{x}(t), \boldsymbol{\theta} | \boldsymbol{y}^o(1{:}\,t-1)) \qquad (10)$$

where $p(\boldsymbol{x}(t), \boldsymbol{\theta}|\boldsymbol{y}^o(1:t))$ is the posterior probability of the state variables $\boldsymbol{x}(t)$ and parameters $\boldsymbol{\theta}$ given all observations up to time t $\boldsymbol{y}^o(1:t)$. The prior knowledge, $p(\boldsymbol{x}(t), \boldsymbol{\theta}|\boldsymbol{y}^o(1:t-1))$, based on the model integration is updated using the likelihood which includes the new observation at time t $p(\boldsymbol{y}^o(t)|\boldsymbol{x}(t), \boldsymbol{\theta})$. In this study, we assumed that our observation error follows Gaussian distribution so that the likelihood can be formulated as follows:

$$p(\boldsymbol{y}^o(t)|\boldsymbol{x}(t), \boldsymbol{\theta}) \equiv L(\boldsymbol{y}^o(t), \boldsymbol{x}(t), \boldsymbol{\theta}) =$$

$$\frac{1}{\sqrt{\det(2\pi\boldsymbol{R})}} \exp\left[-\frac{1}{2}\left(\boldsymbol{y}^o(t) - \boldsymbol{y}^f(t)\right)^T \boldsymbol{R}^{-1}\left(\boldsymbol{y}^o(t) - \boldsymbol{y}^f(t)\right)\right] \quad (11)$$

where $\mathbf{R}$ is the covariance matrix of the observation error process $\boldsymbol{r}(t)$. The prior knowledge of the state variables is approximated by the ensemble simulation:

$$p(\boldsymbol{x}(t)|\boldsymbol{y}^o(1:t-1)) \approx \frac{1}{N}\sum_{i=1}^{N} \delta\left[\boldsymbol{x}(t) - f\left(\boldsymbol{x}^i(t-1), \boldsymbol{\theta}^i, \boldsymbol{u}^i(t-1)\right)\right] \quad (12)$$

where N is the ensemble size, $\boldsymbol{x}^i, \boldsymbol{\theta}^i, \boldsymbol{u}^i$ are the realizations of the ensemble member i, and $\delta[.]$ is the Direc delta function.

The posterior probability of the state variables and parameters can be approximated as follows:

$$p(\boldsymbol{x}(t)|\boldsymbol{y}^o(1:t)) \approx \sum_{i=1}^{N} w(i)\delta(\boldsymbol{x}(t) - \boldsymbol{x}^i(t)) \quad (13)$$

$$p(\boldsymbol{\theta}|\boldsymbol{y}^o(1:t)) \approx \sum_{i=1}^{N} w(i)\delta(\boldsymbol{\theta} - \boldsymbol{\theta}^i) \quad (14)$$

where $w(i)$ is the normalized weight for the realization of the ensemble member i and is calculated using the likelihood (see also equation (11)).

$$w(i) = \frac{L(\boldsymbol{y}^o(t),\boldsymbol{x}^i(t),\theta^i)}{\sum_{k=1}^{N} L(\boldsymbol{y}^o(t),\boldsymbol{x}^k(t),\theta^k)} \quad (15)$$

Note that equations (13) and (14) update all state variables and parameters of the model although the weight is calculated using only observable variables. Therefore, it is not necessary to observe all state variables in order to update all system variables.

The implementation of SIRPF is the following:

1. Model state variables are updated from time t-1 to t using ensemble simulation (equations (8) and (12)).
2. Simulated observations are calculated for all ensembles (equation (9)).
3. The likelihood for each ensemble member is calculated (equation (11))
4. The weights are obtained for all ensembles (equation (15))
5. We applied a resampling procedure according to the normalized weights. The normalized weights of ensemble i, $w(i)$, can be recognized as the probability that the ensemble i is selected after resampling. Resampled state variables and parameters are defined as $\boldsymbol{x}^i_{resamp}$ and $\boldsymbol{\theta}^i_{resamp}$, respectively.

6. Since there are no mechanisms to increase the variance of parameters of ensemble members, Moradkhani et al. (2005) proposed to perturb the ensembles of parameters:

$$\boldsymbol{\theta}^i \leftarrow \boldsymbol{\theta}^i_{resamp} + \varepsilon^i \quad (16)$$

$$\varepsilon^i \sim N(0, \max(\boldsymbol{\omega}, s \times Var^{\theta}) \quad (17)$$

where $N(.)$ is the Gaussian distribution, Var^{θ} is the variance of $\boldsymbol{\theta}^i$, $\boldsymbol{\omega}$ is the fixed hyperparameter (see Table 1 for its variable) which guarantees that the ensembles of parameters do not converge into a single value. s is an adaptively changed factor according to the effective ensemble size, N_{eff}.

$$s = s_0(1 - \left(\frac{N_{eff}}{N}\right)^2) \quad (18)$$

$$N_{eff} = \frac{1}{\sum_{i=1}^{N} w(i)} \quad (19)$$

where $s_0 = 0.05$. The effective ensemble size is the measure of the diversity of ensembles. If the effective ensemble size becomes small, ensembles should be strongly perturbed in order to maintain the diversity of ensembles. Similar strategy has been used in many SIRPF systems (e.g., Moradkhani et al. 2005; Poterjoy et al. 2019).

3. Experiment design

3.1. Observation System Simulation Experiment

In this study, we performed three observation system simulation experiments (OSSEs). In the OSSE, we generated the synthetic truth of the state and flux variables by driving the flood risk model with the specified parameters and input. Then, we generated synthetic observations by adding the noise to this synthetic truth. Those synthetic observations were assimilated into the model by SIRPF. The performance of SIRPF was evaluated by comparing the estimated state variables by SIRPF with the synthetic truth. Model parameters used to generate the synthetic truth can be found in Table 1. They are identical to Di Baldassarre et al. (2013). The OSSE has been recognized as an important preliminary step to verify the newly developed data assimilation systems (e.g., Moradkhani et al. 2005; Vrugt et al. 2013; Penny and Miyoshi 2016; Sawada et al. 2018).

The high water level for the synthetic truth was generated by the following:

$$W = \min(v - 10, 0) \tag{20}$$

v follows the Gumbel distribution:

$$p(v) = \frac{\exp\left(-\frac{v-\mu}{\beta}\right)}{\beta} \exp\left(-\exp(-(v-\mu)\beta)\right) \tag{21}$$

where $\mu = 9, \beta = 2.5$. Although our high water level is not identical to Di Baldassarre et al. (2013), the estimated trajectory of the state variables is similar to Di Baldassarre et al. (2013).

Synthetic observations were generated by adding the Gaussian white noise to the F, G, D, H, and M (see section 2.1) of the synthetic truth. The mean of the Gaussian white noise was 0. The observation error, the standard deviation of the Gaussian white noise, was firstly set to 10% of the synthetic true variables. Although this observation error is generally larger than that used in meteorology and hydrology, we further increased the observation error and tested the sensitivity of the observation error to the SIRPF's performance. We firstly assumed that all of the F, G, D, H, and M can be observed every 10 years or every 10 model integration steps. Then, we evaluated the sensitivity of the observation network (i.e. the observable variables and the observation intervals) to the SIRPF's performance. Although it is not straightforward to observe social memory M, several previous studies obtained the proxy of the social memory by interview data (Barendrecht et al. 2019) and the number of Google searches (Gonzales and Ajami 2017).

We used the ensemble mean of root-mean square errors (mRMSE) as an evaluation metrics:

$$RMSE^i = \sqrt{\frac{1}{T}\sum_{t=1}^{T}(x^i(t) - z(t))} \quad (22)$$

$$mRMSE = \frac{1}{N}\sum_{i=1}^{N} RMSE^i \quad (23)$$

where $RMSE^i$ is root-mean-square-error for i th ensemble, T is the computational period, $x^i(t)$ is the simulated state variables of ensemble i at time t, $z(t)$ is the synthetic truth at time t.

3.1.1. Experiment 1: Perfect model with uncertain high water levels

In the first OSSE, we assumed that there is no uncertainty in model parameters. We used the same parameter variables as the synthetic truth run and we did not perform the estimation of parameters. Our SIRPF updated only state variables. Although the model had no uncertainty, it was assumed that the input data, the timeseries of the high water level, were uncertain. Lognormal multiplicative noise was added to the synthetic true high water level so that different ensemble members have different high water levels in the data assimilation experiment. The two parameters of the lognormal distribution, commonly called μ and σ, were set to 0 and 0.15, respectively.

3.1.2. Experiment 2: Unknown model parameters and uncertain high water levels

In the second OSSE, we assumed that some of the synthetic true parameter values were unknown. The unknown parameters in the experiment 2 were the cost of levee raising γ_E, the rate by which new properties can be built φ_P, the rate of decay of levees κ_T, and memory loss rate μ_S (see Table 1). We selected these unknown parameters one by one from four equations of economy, politics, technology, and social to discuss how each state variable's observation affects the estimation of parameters across these four equations (see section 2.1). We have no unknown parameters related to F (equation (1)) since it is unlikely that the parameters in equation (1) are much more inaccurate than the other parameters. The parameters related to flood are mainly determined by the topography of the flood plain so that the process described in equation (1) can be replaced by more accurate hydrodynamic models in the real-world case study. The initial parameter variables were assumed to be distributed in the bounded uniform distributions whose ranges were found in Table 1. The uncertainty of the simulation induced by these parameters' uncertainty is large enough to demonstrate the potential of data assimilation to minimize the simulation's uncertainty (see Results). Our SIRPF sequentially assimilated observations and estimated both state variables and parameters in the experiment 2. The high water level data were uncertain as the experiment 1.

3.1.3. Experiment 3: Unknown and time-variant model parameters and uncertain high water levels

To further demonstrate the potential of sequential data assimilation in socio-hydrology, we assumed that the description of the model was biased in the experiment 3. Here we assumed that two of the model parameters were temporally varied by the unknown dynamics. Specifically, the rate by which new properties can be built, φ_P, and the memory loss rate, μ_S, were temporally varied in the experiment 3:

$$\varphi_P(t) = \begin{cases} 5000 \ (t < 250) \\ 5000 + (t - 250) \times \frac{40000-5000}{500} (250 \leq t < 750) \\ 40000 \ (750 \leq t) \end{cases} \quad (24)$$

$$\mu_S(t) = \begin{cases} 0.01 \ (t < 250) \\ 0.01 + (t - 250) \times \frac{0.10-0.01}{500} \ (250 \leq t < 750) \\ 0.10 \ (750 \leq t) \end{cases} \quad (25)$$

In the data assimilation experiment, we assumed that the dynamics of φ_P and μ_S was unknown, and we integrated the flood risk model with time-invariant φ_P and μ_S. We evaluated if SIRPF could track this time-variant parameter and reveal the bias of the model's description. The cost of levee raising γ_E, and the rate of decay of levees κ_T

were assumed to be time-invariant unknown parameters as they were in the experiment 2. The cost of levee raising γ_E affects the state variables of the flood risk model mainly in the initial early years and the gradual change of the rate of decay of levees κ_T has few impacts on the state variables. Therefore, we found that it is difficult to track the temporal change of these two parameters. The input forcing data, high water level, were uncertain as described in the experiment 1.

3.2. Real-data experiment

In addition to the OSSEs, we performed the real-world experiment in the city of Rome, Italy. Ciullo et al. (2017) collected real-world data and calibrated their flood risk model. Using the data collected by Ciullo et al. (2017), we performed the data assimilation experiment. It should be noted that the flood risk model of Ciullo et al. (2017) is different from our model (i.e. Di Baldassarre et al. 2013), although they are conceptually similar.

All the data were collected from Figure 1 of Ciullo et al. (2017) by WebPlotDigitizer (https://automeris.io/WebPlotDigitizer/). The observed high water level of Tiber River was used as input forcing data (W). The levee height (H) and population (G) were used as the observation data to be assimilated into the flood risk model. In Ciullo et al. (2017), population values within the Tiber's floodplain were normalized by the theoretical maximum Tiber's floodplain population which is estimated to the range between 10^6 and 2×10^6. Since our flood risk model needs the population values (not normalized values), we multiplied 1.5×10^6 and the normalized values shown in Figure 1 of Ciullo et al. (2017) to obtain population in the floodplain.

We added lognormal multiplicative noise to the observed high water level as we did in the OSSEs. The observation errors of levee height and population were set to 10% and 25% of the observed values, respectively. Since Ciullo et al. (2017) showed the large uncertainty in the estimation of the theoretical maximum population (see above), it is reasonable to assume that the estimation of population values also has relatively large uncertainty.

As the second and third OSSEs, we have 4 unknown parameters in this real-world experiment. We used the same settings of parameters as the OSSEs, which are shown in Table 1, except for ξ_H, proportion of additional high water level due to levee heightening. In this real-world experiment, we set $\xi_H = 0$ because the observed high water level includes the effects of levee heightening. This treatment is consistent to Ciullo et al. (2017) (see their Table 2).

The initial conditions of H and M were set to 0. The initial conditions of D were obtained from the uniform distribution between 1000 and 5000. The initial conditions of G were obtained from the uniform distribution between 1500 and 50000.

4. Results

4.1. Observation System Simulation Experiment

4.1.1. Experiment 1: Perfect model with uncertain high water levels

Figure 1 shows the timeseries of the model variables calculated by 5000 ensembles with no data assimilation. Although the ensemble mean of the state variables is close to the synthetic truth, the ensembles have the large spread especially for G. The uncertainty in the input forcing brings the uncertainty in the estimation of the historical socio-hydrologic condition.

Figure 2 indicates that this uncertainty is mitigated by assimilating the observations of F, G, D, H, and M into the model every 10 years with 5000 ensembles. Table 2 shows that RMSE is reduced for all state variables by data assimilation.

While we can observe all of F, G, D, H, and M in Figure 2 and Table 2, Figure 3 shows the performance of our SIRPF in which only one of them can be observed. Our SIRPF updates all state variables although only one of them is assimilated. Figure 3 reveals that we can accurately propagate the observation information into the model state space. In other words, our SIRPF can positively impact the estimation of not only observed state variables but unobserved state variables. For instance, even if we can observe only G, the simulation of all G, D, H, and M is improved. This finding is promising since all of the state variables cannot be observed in the real-world applications. Figure 3 also shows that observing F is not effective compared with the other variables. This is because F is a flux and F can be observed only when floods occur so that the number of effective observations is small. In addition, observing F, D, and M negatively impacts the estimation of H and observing H does not significantly improve the simulation of D and M. Although the dynamics of F, D, and M strongly affects the decision making of whether the levees are raised or not, the amount by which the levees are raised, R, is fully determined by the high water level, W, once the community determines to raise the levees (see equation (2)). Therefore, the uncertainty of H is largely induced by the uncertainty of the high water level, W, whose uncertainty is not directly mitigated by our SIRPF. This is why observing F, D, and M is not helpful to mitigate the uncertainty of H.

While we can observe every 10 years in Figure 2 and Table 2, Figure 4 shows the sensitivity of the observation intervals to the performance of our SIRPF. Our SIRPF improves the estimation of the state variables when we can obtain observation once in 50-year or 100-year (see also Figure S1 for timeseries of the model's variables), which is promising since we cannot expect the frequent observations in the real-world applications.

We set the observation error to 10% of the synthetic truth thus far. The improvement of the simulation skill can be found with larger observation errors (Figure S2). Although the SIRPF's performance gradually declines as the observation error increases, our SIRPF can significantly improve the simulation skill with 25% observation error.

Although we demonstrate the potential of our SIRPF with 5000 ensembles thus far, the improvement of the simulation skill can be found in much smaller ensemble sizes. The performance of our SIRPF with 20 ensembles is similar to that with 5000 ensembles (Figure S3).

4.1.2. Experiment 2: Unknown model parameters and uncertain high water levels

Figure 5 reveals that the flood risk model completely loses its skill to estimate the human-flood interactions if there are uncertainties in model parameters and high water levels prescribed in Section 3. In contrast to the experiment 1, the ensemble mean cannot accurately reproduce the synthetic truth.

Figure 6 indicates that our SIRPF can accurately estimate the model state variables by assimilating the observations of F, G, D, H, and M into the model every 10 years with 5000 ensembles. Figure 7 indicates that four unknown parameters can also be accurately estimated. We find that it is relatively difficult to estimate the rate of levee's decay, κ_T, compared with the other parameters. This is because κ_T strongly affects the dynamics of H and the uncertainty in H is largely determined by the uncertainty in high water levels, which is not directly mitigated by our SIRPF system. Table 3 shows that RMSE is reduced for both state variables and parameters by data assimilation.

We analyzed the impacts of the individual observation types on the simulation skill as we did in the experiment 1. Figure 8a shows that the effects of the individual observation types are similar to what we found in the experiment 1: (1) our SIRPF can improve the skill to simulate unobservable state variables; (2) observing F is not effective compared with the other observations; (3) observing H does not significantly improve the simulation of D and M. Figure 8b reveals that the parameters can be efficiently estimated by assimilating the observation of the state variables which are tightly related to the targeted parameters. For instance, observing D can greatly improve the rate by which new properties can be built, φ_P, in equation (5) which governs the dynamics of D. However, assimilating a single observation type can contribute to accurately estimating all four parameters in many cases, which is the promising result considering the sparsity of the observation in the real-world applications.

The good performance of our SIRPF can be found with the longer observation intervals as we found in the experiment 1. Figure 9 indicates that our SIRPF can improve the estimation of the state variables and parameters when we can obtain observation once in 50-year or 100-year (see also Figures S4 and S5 for timeseries of the model's variables).

As we found in the experiment 1, the SIRPF's performance declines with the increased observation error (Figure S6). However, it is promising that our SIRPF can improve the simulation skill with larger observation errors up to 25% of the synthetic truth considering that the observations in the socio-hydrologic domain are often inaccurate.

In contrast to the experiment 1, the larger ensemble size is required to stably estimate both state variables and parameters (Figure S7). The increased degree of freedom and the nonlinear relationship between parameters and observations increase the necessary ensemble size.

4.1.3. Experiment 3: Unknown and time-variant model parameters and uncertain high water levels

In addition to the experiment 2, two of the unknown parameters (φ_P and μ_S) temporally vary in the synthetic truth of the experiment 3. We found that a larger spread of φ_P is required to stably track the time-variant synthetic true φ_P so that we increased s_0 in equation (18) from 0.05 to 0.5 only for φ_P in this experiment 3. Figure 10 and Table 4 indicate that despite the error in the model's description, our SIRPF can greatly improve the simulation of the flood risk model. Please note that the synthetic truth shown in Figure 10 is different from that of the previous experiments especially for D and M. Figures 11b and 11d indicate that we can accurately estimate the time-variant parameters (φ_P and μ_S) as well as the other time-invariant parameters (Figures 11a and 11c). This result is promising since we cannot expect the perfect description of the socio-hydrologic model in the real-world applications. We also performed the sensitivity test on observation types, observation intervals, and ensemble sizes, which results in the same conclusions as the experiment 2 (not shown).

4.2. Real-data experiment

Figure 12 shows the timeseries of the model variables calculated by 5000 ensembles with no data assimilation. The 5000-ensemble simulation reveals the two bifurcated social systems. One builds a high levee and maintains a course of stable economic growth. The other one has no levee and its economy is damaged by severe floods many times (ensemble mean shown in Figure 12b implies that there are many ensemble members with zero levee height).

In reality, the city of Rome constructed the levee responding to the severe flood occurred on 28 December 1870. After the construction of this levee, no major flood losses occurred, allowing the steady and undisturbed growth. Figure 13 indicates that our SIRPF successfully constrains the trajectory of the ensemble simulation to the real-world (i.e. high levee and stable economic growth) by assimilating the real data of H and G. Figure S8 shows the SIRPF-estimated unknown parameters. Our SIRPF suggests lower γ_E than the initial ensemble mean to promote the levee construction with lower costs. Lower κ_T is also obtained because the assimilated real data show no decay of levee from 1874 to 2009. Compared with the OSSE experiment 2, the large uncertainty in estimated parameters remains at the final timestep due to the limited number of assimilated observations. In contrast to the OSSEs, our observation network has the uneven temporal distribution. Figure 13 clearly indicates that our SIRPF is robust to these intermittent observations whose intervals temporally change.

We analyzed the impacts of the individual observation types (i.e. H and G) on the simulation skill as we did in the OSSEs. Figure 14 indicates that our SIRPF realistically simulates the socio-hydrologic dynamics in the city of Rome and provides the similar estimated state variables shown in Figure 13 by assimilating only population data. As we found in the OSSEs, observations of the size of the human settlement G are informative to effectively constrain the flood risk model. The dynamics of the parameter estimation is similar to the case in which data of both G and H are assimilated (Figure S9).

On the other hand, assimilating only levee height data cannot provide the similar results to those shown above. Figure 15 shows the timeseries of the model variables by the data assimilation experiment in which we assimilated the observation data of H only. Observations of the levee height cannot effectively constrain D, G, and M compared with the observations of G. This finding is consistent to the OSSEs. The uncertainty in estimated parameters becomes larger when we omit to assimilate observations of G (Figure S10). Although the impact of levee height data is limited compared with population data, it is promising that we can estimate the socio-hydrologic dynamics to some extent only from the levee height data whose distribution is temporally sparse.

5. Discussion

In this study, we developed the sequential data assimilation system for the widely adopted socio-hydrological model, the flood risk model by Di Baldassarre et al. (2013). We demonstrated that our SIRPF for the flood risk model is useful to reconstruct the historical human-flood interactions, which can be called "socio-hydrologic reanalysis", by integrating sparsely distributed observations and imperfect numerical simulation. Our idealized OSSE and real-data experiment reveal several important findings.

First, the sequential data assimilation can mitigate the negative impact of the uncertainty in the input forcing on the simulation of socio-hydrologic state variables. We found that the small perturbation of high water levels greatly affects the long-term trajectory of the socio-hydrologic state variables as Viglione et al. (2014) found. It is necessary to sequentially constrain the state variables and parameters by sequential data assimilation if the input forcing is uncertain although previous studies on the model-data integration in socio-hydrology mainly focused on parameter calibration assuming no uncertainty in the input forcing (e.g., Barendrecht et al. 2019; Roobavannan et al. 2017; Ciullo et al. 2017; van Emmerik et al. 2014; Gonzales and Ajami 2017). To deeply understand the socio-hydrologic processes, the long-term historical analysis should be performed. Although there are many studies on the accurate reconstruction of the historical weather condition (e.g., Toride et al. 2017), it may be necessary to tackle with the uncertainty in hydrometeorological datasets used for the input forcing of the socio-hydrologic models.

Second, our SIRPF can efficiently improve the simulation of the socio-hydrologic state variables using the sparsely distributed data. All model variables should not necessarily be observed to constrain the model's state variables and parameters. In some cases, observations of a single state variable are enough to reconstruct the accurate socio-hydrologic state. In addition, observation intervals can be longer than 10-year. Since it is difficult to obtain the large volume of data in socio-hydrology, this finding is promising. We also give some insights about the informative observation types in the flood risk model. With uncertain high water levels, observations of the intensity of flooding events F and the height of levee H are not informative (i.e. the assimilation of these observations cannot greatly improve the simulation skill) although the empirical data which can be related to F and H may be easily found. On the other hand, observations of the size of the human settlement G are informative to constrain the flood risk model. Model parameters can be efficiently estimated by assimilating the state variables which is tightly related to the targeted parameters, which is consistent to the findings of the idealized experiment by Barendrecht et al. (2019).

Third, our SIRPF is robust to the imperfectness of the socio-hydrologic model. The unknown parameters can be efficiently estimated by the sequential data assimilation. While previous studies evaluated the trajectory in the whole study period to calibrate the socio-hydrologic models by iteratively performing the long-term model integration (e.g., Barendrecht et al. 2019; Roobavannan et al. 2017; Ciullo et al. 2017; van Emmerik et al. 2014; Gonzales and Ajami 2017), we sequentially optimize parameters based on the relatively short-term timeseries allowing parameters to temporally vary in the study period. The advantage of this strategy is that we can deal with time-variant parameters as previously demonstrated in the applications to hydrologic models (e.g., Pathiraja et al. 2018). In the model development, parameters are formulated as time-invariant values so that the existence of time-variant parameters indicates the imperfect description of dynamic models. Sequential data assimilation can mitigate the negative impact of this imperfect model description. Vrugt et al. (2013) pointed out that the parameter optimization by the sequential filters is unstable if parameter sensitivity temporally changes (e.g., parameters affects the model's dynamics differently in the different seasons), which may be the potential limitation of our strategy compared with Bayesian inference based on the long-term trajectory such as Barendrecht et al. (2019).

6. Conclusion

In this study, we proposed to apply the sequential data assimilation to the socio-hydrologic models. By several OSSEs and the real-data experiment in the flood risk modeling, we found that our proposed SIRPF is robust to the imperfect input forcing and the imperfect model. The sequential data assimilation is useful to reconstruct the socio-hydrologic conditions from the inaccurate and sparsely distributed data and the imperfect simulation.

Acknowledgements

We thank Di Baldassarre for sharing the original source code of the flood risk model. We thank two anonymous referees for their constructive comments. Data Integration and Analysis System (DIAS) provided us the computational resources.

Code/Data availability

Code and data are available upon the request to the corresponding author.

Author Contribution

YS designed the study. RH and YS jointly developed the data assimilation system for the flood risk model and performed the numerical experiments. YS and RH contributed to interpreting the results. YS wrote the first draft of the paper and RH contributed to editing the paper.

Competing interests

The authors declare that they have no conflict of interest.

References

Barendrecht, M. H., Viglione, A., Kreibich, H., Merz, B., Vorogushyn, S., and Blöschl, G.: The Value of Empirical Data for Estimating the Parameters of a Sociohydrological Flood Risk Model. *Water Resources Research*. https://doi.org/10.1029/2018WR024128, 2019

Bauer, P., Thorpe, A., and Brunet, G.: The quiet revolution of numerical weather prediction. *Nature*, *525*(7567), 47–55. https://doi.org/10.1038/nature14956, 2015

Ciullo, A., Viglione, A., Castellarin, A., Crisci, M., and Di Baldassarre, G.: Socio-hydrological modelling of flood-risk dynamics: comparing the resilience of green and technological systems. *Hydrological Sciences Journal*, *62*(6), 880–891. https://doi.org/10.1080/02626667.2016.1273527, 2017

Dang, Q., and Konar, M.: Trade Openness and Domestic Water Use. *Water Resources Research*, *54*(1), 4–18. https://doi.org/10.1002/2017WR021102, 2018

Di Baldassarre, G., Viglione, A., Carr, G., Kuil, L., Salinas, J. L., and Blöschl, G.: Socio-hydrology: Conceptualising human-flood interactions. *Hydrology and Earth System Sciences*, *17*(8), 3295–3303. https://doi.org/10.5194/hess-17-3295-2013, 2013

Di Baldassarre, G., et al.: Socio-hydrology: Scientific Challenges in Addressing a Societal Grand Challenge. *Water Resources Research*, 1–29. https://doi.org/10.1029/2018wr023901, 2019

Gonzales, P., and Ajami, N.: Social and Structural Patterns of Drought-Related Water Conservation and Rebound. *Water Resources Research*, *53*(12), 10619–10634. https://doi.org/10.1002/2017WR021852, 2017

Hersbach, H. et al.: Global reanalysis: goodbye ERA-Interim, hello ERA5, *ECMWF Newsletter, 159,* 17-24, doi: 10.21957/vf291hehd7, 2019

Kobayashi, S., et al.: The JRA-55 Reanalysis: General Specifications and Basic Characteristics. *Journal of the Meteorological Society of Japan, 93,* 5-48. https://doi.org/10.2151/jmsj.2015-001, 2015

Kreibich, H., et al.: Adaptation to flood risk: Results of international paired flood event studies. *Earth's Future*. https://doi.org/10.1002/eft2.232, 2017

Lievens, H., et al.: Joint Sentinel-1 and SMAP data assimilation to improve soil moisture estimates. *Geophysical Research Letters*, *44*(12), 6145–6153. https://doi.org/10.1002/2017GL073904, 2017

Miyoshi, T., and Yamane, S.: Local Ensemble Transform Kalman Filtering with an AGCM at a T159/L48 Resolution. *Monthly Weather Review*, *135*(2002), 3841–3861. https://doi.org/10.1175/2007MWR1873.1, 2007

Moradkhani, H., Hsu, K. L., Gupta, H., and Sorooshian, S.: Uncertainty assessment of hydrologic model states and parameters: Sequential data assimilation using the particle filter. *Water Resources Research*, *41*(5), 1–17. https://doi.org/10.1029/2004WR003604, 2005

Mostert, E.: An alternative approach for socio-hydrology: Case study research. *Hydrology and Earth System Sciences*, *22*(1), 317–329. https://doi.org/10.5194/hess-22-317-2018, 2018

Mount, N., J., et al.: Data-driven modelling approaches for sociohydrology: opportunities and challenges within the Panta Rhei Science Plan. *Hydrological Sciences Journal, 61(7),* 1192-1208. https://doi.org/10.1080/02626667.2016.1159683, 2016

Pande, S., and Savenije, H. H. G.: A sociohydrological model for smallholder farmers in Maharashtra, India. *Water Resources Research*, *52*(3), 1923–1947. https://doi.org/10.1002/2015WR017841, 2016

Pathiraja, S., Anghileri, D., Burlando, P., Sharma, A., Marshall, L., and Moradkhani, H.: Time-varying parameter models for catchments with land use change: the importance of model structure, Hydrol. Earth Syst. Sci., *22*, 2903–2919, https://doi.org/10.5194/hess-22-2903-2018, 2018.

Penny, S. G., and Miyoshi, T.: *A local particle filter for high-dimensional geophysical systems*. 391–405. https://doi.org/10.5194/npg-23-391-2016, 2016

Poterjoy, J., Wicker, L., and Buehner, M.: Progress toward the application of a localized particle filter for numerical weather prediction. *Monthly Weather Review*, *147*(4), 1107–1126. https://doi.org/10.1175/MWR-D-17-0344.1, 2019

Qin, J., Liang, S., Yang, K., Kaihotsu, I., Liu, R., and Koike, T.: Simultaneous estimation of both soil moisture and model parameters using particle filtering method through the assimilation of microwave signal. *Journal of Geophysical Research*, *114*(D15), 1–13. https://doi.org/10.1029/2008JD011358, 2009

Rasmussen, J., Madsen, H., Jensen, K. H., and Refsgaard, J. C.: Data assimilation in integrated hydrological modeling using ensemble Kalman filtering: evaluating the effect of ensemble size and localization on filter performance. *Hydrology and Earth System Sciences*, *19*(7), 2999–3013. https://doi.org/10.5194/hess-19-2999-2015, 2015

Roobavannan, M., Kandasamy, J., Pande, S., Vigneswaran, S., and Sivapalan, M.: Role of Sectoral Transformation in the Evolution of Water Management Norms in Agricultural Catchments: A Sociohydrologic Modeling Analysis. *Water Resources Research*, *53*(10), 8344–8365. https://doi.org/10.1002/2017WR020671, 2017

Sawada, Y., Koike, T., and Walker, J. P.: A land data assimilation system for simultaneous simulation of soil moisture and vegetation dynamics. *J. Geophys. Res. Atmos.*, *120*, 5910– 5930. doi: 10.1002/2014JD022895, 2015

Sawada, Y., Nakaegawa, T. and Miyoshi, T.: Hydrometeorology as an inversion problem: Can river discharge observations improve the atmosphere by ensemble data assimilation? *Journal of Geophysical Research: Atmospheres*, 123, 848– 860. https://doi.org/10.1002/2017JD027531, 2018

Sawada, Y., Okamoto, K., Kunii, M., and Miyoshi, T.: Assimilating every-10-minute Himawari-8 infrared radiances to improve convective predictability. *Journal of Geophysical Research: Atmospheres*, 124, 2546–2561. https://doi.org/10.1029/2018JD029643, 2019

Sivapalan, M., Savenije, H.H.G. and Blöschl, G.: Socio-hydrology: A new science of people and water. Hydrol. Process., 26: 1270-1276. doi:10.1002/hyp.8426, 2012

Sivapalan, M., Konar, M., Srinivasan, V., Chhatre, A., Wutich, A., Scott, C. A., and Wescoat, J. L.: Socio-hydrology: Use-inspired water sustainability science for the Anthropocene, *Earth's Future*, *2*, 225–230. https://doi.org/10.1002/2013EF000164, 2014.

Toride, K., Neluwala, P., Kim, H. and Yoshimura, K.: Feasibility Study of the Reconstruction of Historical Weather with Data Assimilation. *Mon. Wea. Rev.,* **145**, 3563–3580, https://doi.org/10.1175/MWR-D-16-0288.1, 2017

Van Emmerik, T. H. M., et al.: Socio-hydrologic modeling to understand and mediate the competition for water between agriculture development and environmental health: Murrumbidgee River basin, Australia. Hydrology and Earth System Sciences, 18(10), 4239–4259. https://doi.org/10.5194/hess-18-4239-2014, 2014

Viglione, A., et al.: Insights from socio-hydrology modelling on dealing with flood risk - Roles of collective memory, risk-taking attitude and trust. *Journal of Hydrology*, *518*(PA), 71–82. https://doi.org/10.1016/j.jhydrol.2014.01.018, 2014

Vrugt, J. A., ter Braak, C. J. F., Diks, C. G. H., and Schoups, G.: Hydrologic data assimilation using particle Markov chain Monte Carlo simulation: Theory, concepts and applications. *Advances in Water Resources*, *51*, 457–478. https://doi.org/10.1016/j.advwatres.2012.04.002, 2013

Yu, D. J., Sangwan, N., Sung, K., Chen, X., and Merwade, V.: Incorporating institutions and collective action into a sociohydrological model of flood resilience. *Water Resources Research*, *53*(2), 1336–1353. https://doi.org/10.1002/2016WR019746, 2017

Table 1. Parameters of the flood risk model

	description	Values	Ranges in data assimilation	$\boldsymbol{\omega}$ in equation (17)
$\boldsymbol{\xi_H}$	proportion of additional high water level due to levee heightening	0.5	-	-
$\boldsymbol{\alpha_H}$	parameter related to the slope of the floodplain and the resilience of the human settlement	0.01	-	-
$\boldsymbol{\rho_E}$	maximum relative growth rate	0.02	-	-
$\boldsymbol{\lambda_E}$	critical distance from the river beyond which the settlement can no longer grow	5000	-	-
$\boldsymbol{\gamma_E}$	Cost of levee raising	0.5	0.2-5.0	0.01
$\boldsymbol{\lambda_P}$	distance at which people would accept to live when they remember past floods whose total consequences were perceived as a total destruction of the settlement	12000	-	
$\boldsymbol{\varphi_P}$	rate by which new properties can be built	10000	1000-50000	100
$\boldsymbol{\varepsilon_T}$	safety factor for levees rising	1.1	-	-
$\boldsymbol{\kappa_T}$	rate of decay of levees	0.001	0-0.0015	0.0000025
$\boldsymbol{\alpha_S}$	proportion of shock after flooding if levees are risen	0.5	-	-
$\boldsymbol{\mu_S}$	memory loss rate	0.05	0-0.4	0.0025

Table 2. RMSE of the no data assimilation experiment (NoDA) and the data assimilation experiment (DA) in which all observations are assimilated every 10 years with 5000 ensembles in the experiment 1 (see section 3.1).

	NoDA	DA
G	1.06×10^{6}	1.64×10^{4}
D	3.60×10^{2}	3.92×10^{1}
H	2.65	1.41
M	1.08×10^{-1}	8.32×10^{-2}

Table 3. RMSE of the no data assimilation experiment (NoDA) and the data assimilation experiment (DA) in which all observations are assimilated every 10 years with 5000 ensembles in the experiment 2 (see section 3.2).

	NoDA	DA
G	2.97×10^{6}	1.64×10^{4}
D	1.86×10^{3}	1.01×10^{2}
H	9.35	1.63
M	2.24×10^{-1}	8.99×10^{-2}
γ_E	2.08	4.27×10^{-1}
φ_P	1.72×10^{4}	3.81×10^{3}
κ_T	4.12×10^{-4}	2.36×10^{-4}
μ_S	1.55×10^{-1}	2.43×10^{-2}

Table 4. RMSE of the no data assimilation experiment (NoDA) and the data assimilation experiment (DA) in which all observations are assimilated every 10 years with 5000 ensembles in the experiment 3 (see section 3.3).

	NoDA	DA
G	2.91×10^{6}	6.20×10^{3}
D	2.20×10^{3}	2.02×10^{2}
H	9.21	1.65
M	2.48×10^{-1}	1.05×10^{-1}
γ_E	2.08	5.20×10^{-1}
φ_P	1.98×10^{4}	7.68×10^{3}
κ_T	4.12×10^{-4}	2.54×10^{-4}
μ_S	1.60×10^{-1}	3.03×10^{-2}

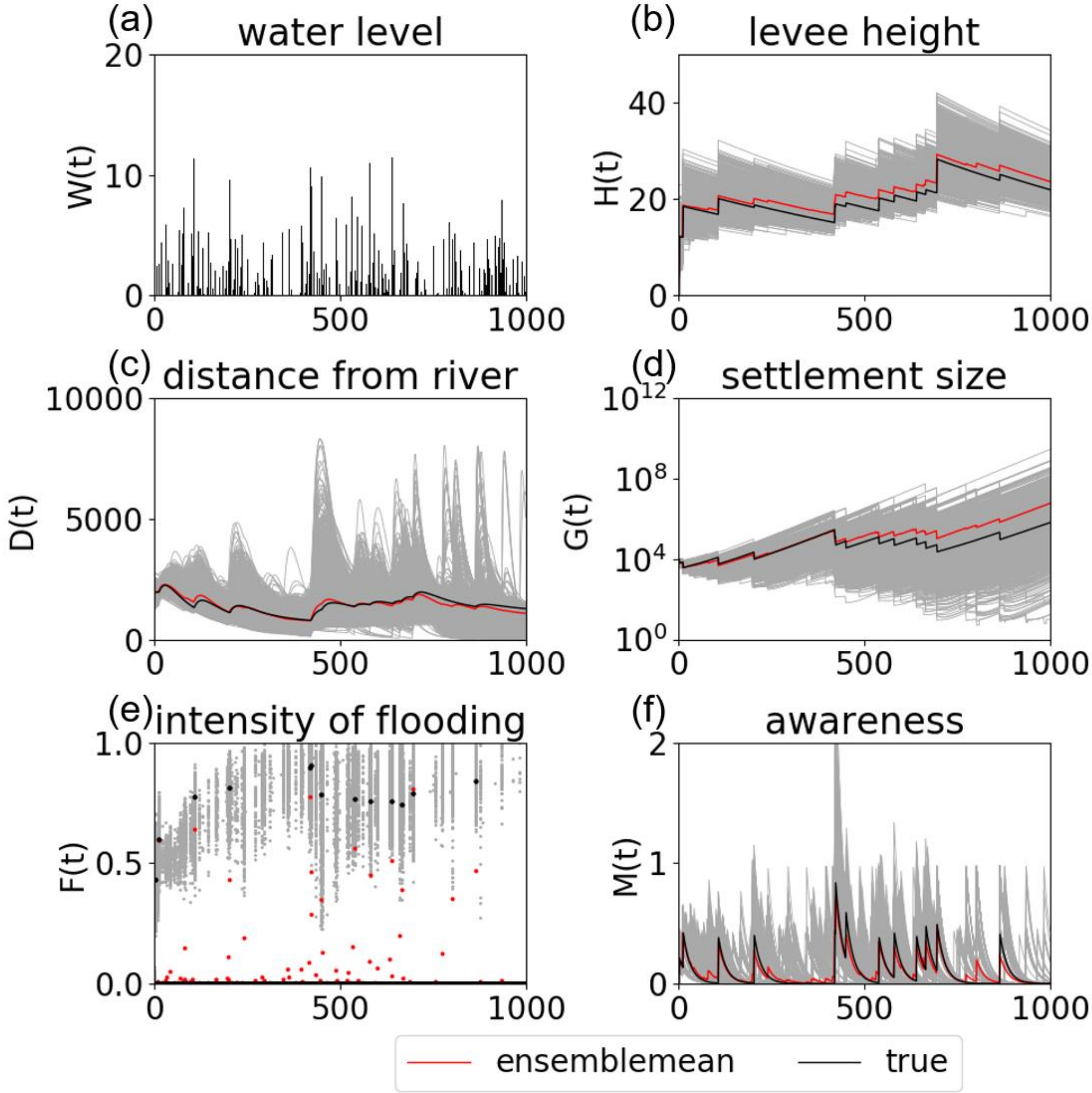

Figure 1. Timeseries of (a) high water level W(t), (b) the flood protection level (or levee height) H(t), (c) the distance of the center of mass of the human settlement from the river D(t), (d) the size of the human settlement G(t), (e) the intensity of flooding events F(t), and (f) the social awareness of the flood risk M(t) simulated by 5000 ensembles with uncertain high water levels and no data assimilation in the experiment 1 (see section 3.1.1). The time step is annual. Grey, red, and black lines are the ensemble members, their mean, and the synthetic truth, respectively.

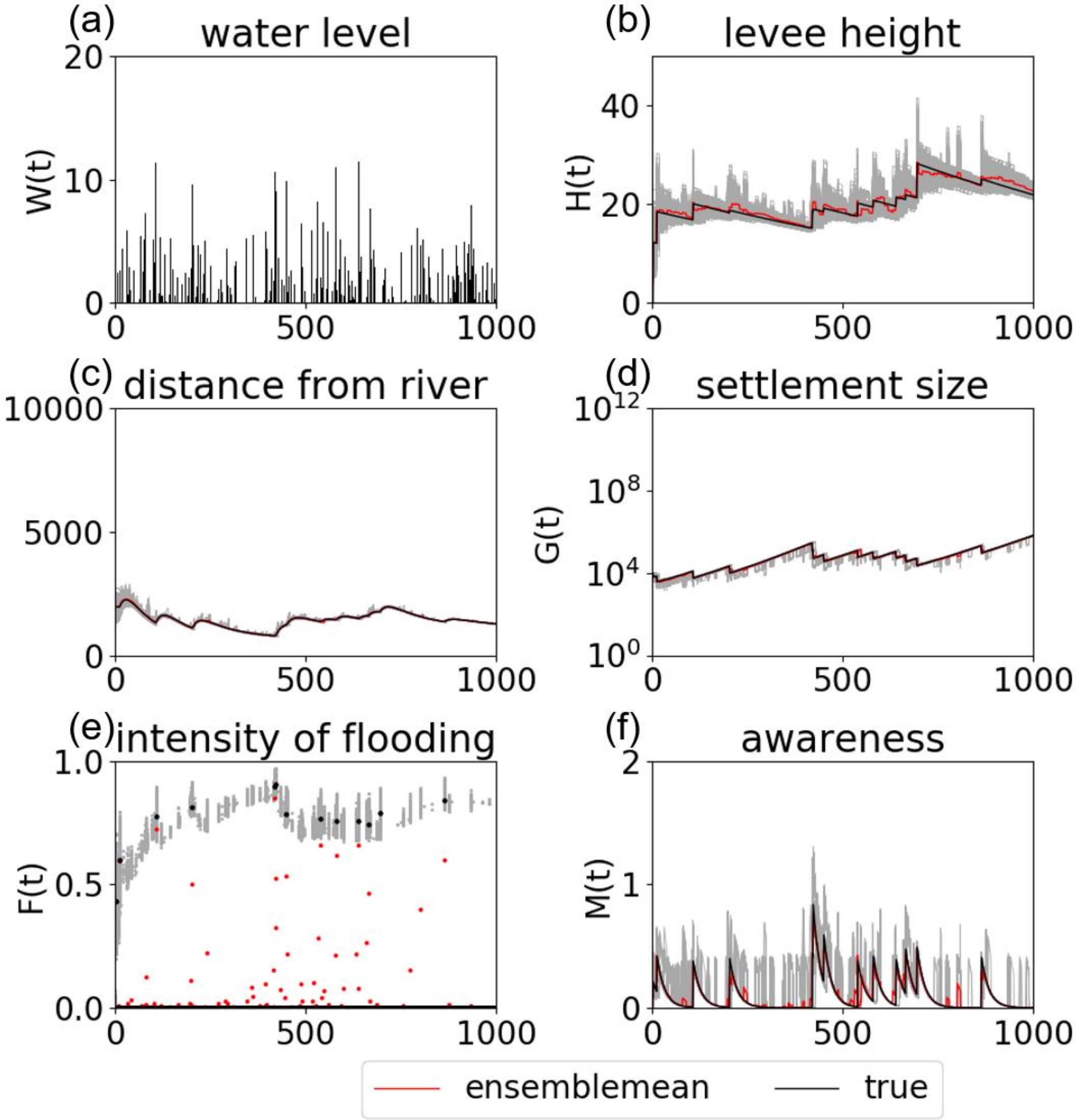

Figure 2. Timeseries of (a) high water level W(t), (b) the flood protection level (or levee height) H(t), (c) the distance of the center of mass of the human settlement from the river D(t), (d) the size of the human settlement G(t), (e) the intensity of flooding events F(t), and (f) the social awareness of the flood risk M(t) simulated by the data assimilation experiment in which the observations of F, G, D, H, and M are assimilated into the model

every 10 years with 5000 ensembles in the experiment 1 (see section 3.1.1). The time step is annual. Grey, red, and black lines are the ensemble members, their mean, and the synthetic truth, respectively.

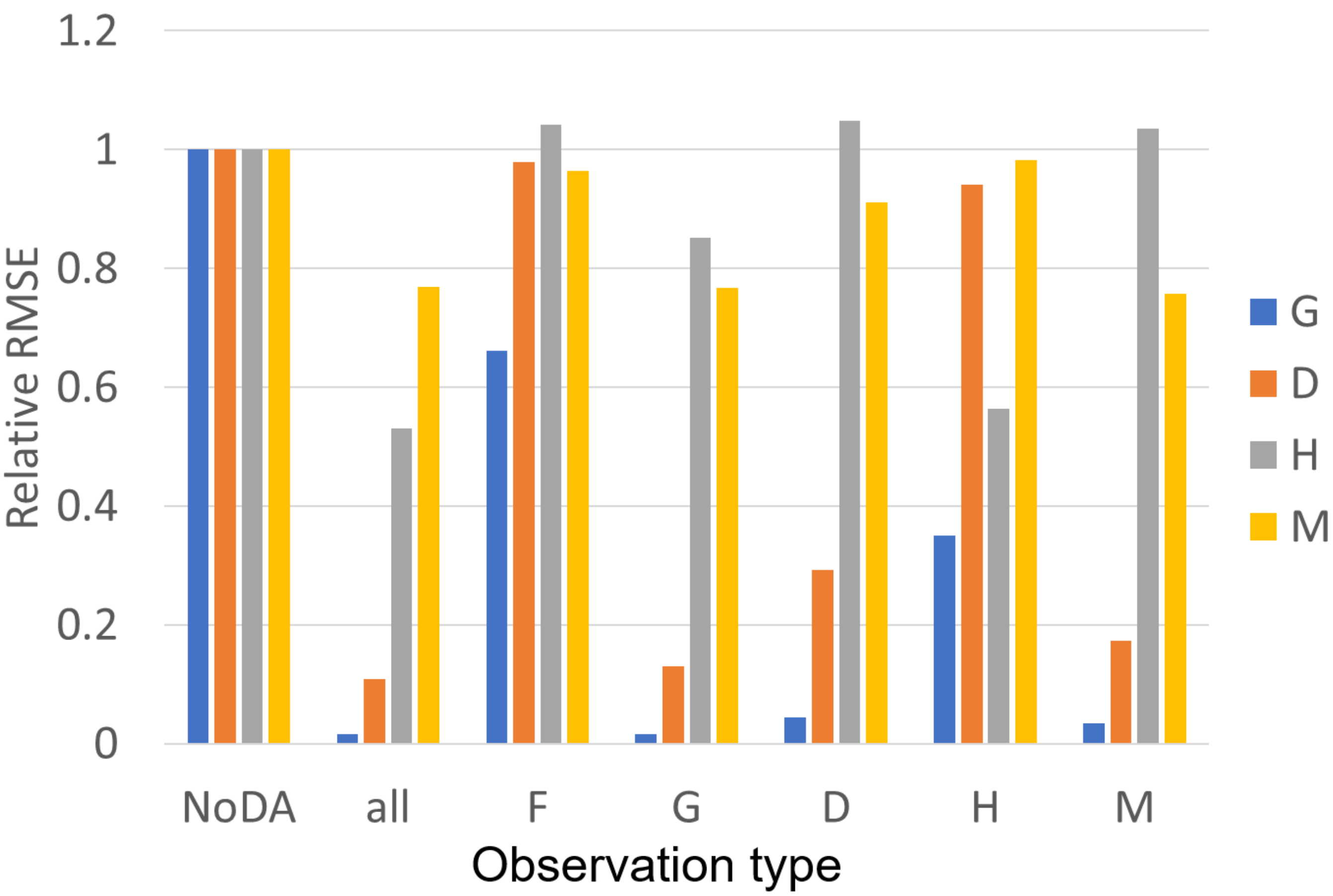

Figure 3. The ratio of RMSEs of the no data assimilation experiment (NoDA) to those of the data assimilation experiments in which all of observations (F, G, D, H, and M) are assimilated (all) and each one of them is assimilated in the experiment 1 (see section 3.1.1). Blue, orange, gray, and yellow bars are RMSEs of the size of the human settlement G(t), the center of mass of the human settlement from the river D(t), the flood protection level (or levee height) H(t), and the social awareness of the flood risk M(t).

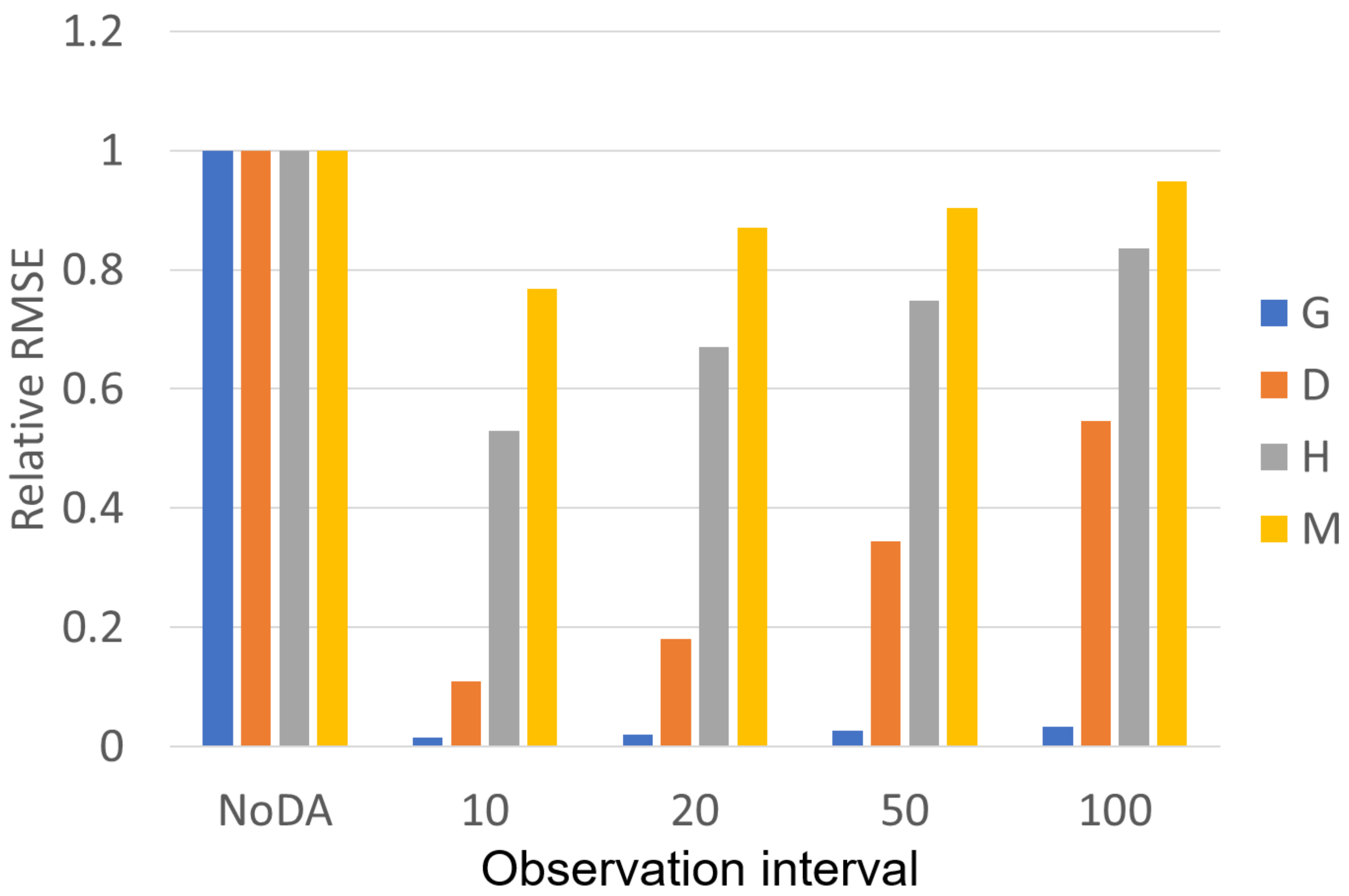

Figure 4. The ratio of RMSEs of the no data assimilation experiment (NoDA) to those of the data assimilation experiments in which all of observations (F, G, D, H, and M) are assimilated every 10, 20, 50, and 100 years in the experiment 1 (see section 3.1.1). Blue, orange, gray, and yellow bars are RMSEs of the size of the human settlement G(t), the center of mass of the human settlement from the river D(t), the flood protection level (or levee height) H(t), and the social awareness of the flood risk M(t).

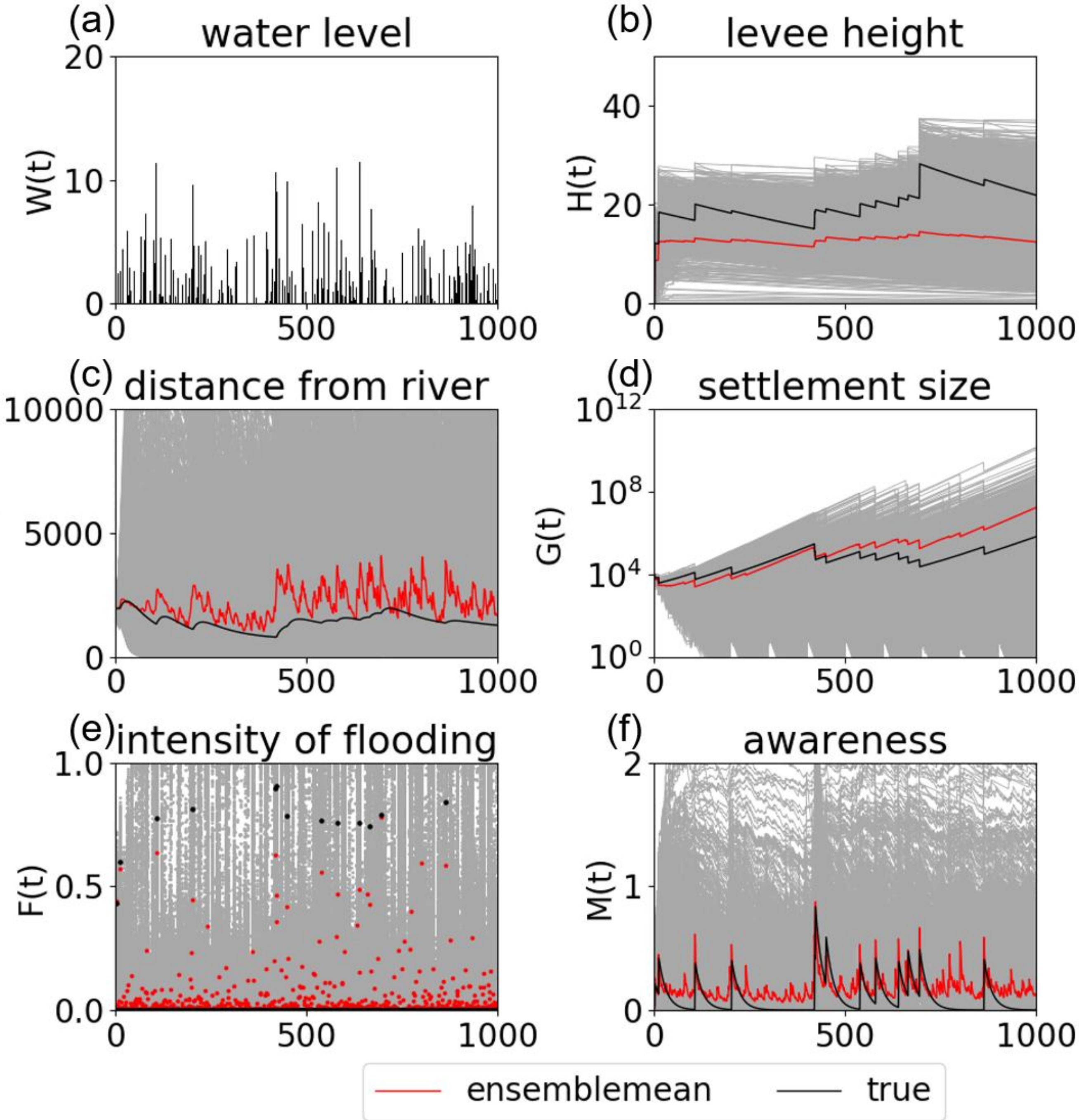

Figure 5. Timeseries of (a) high water level W(t), (b) the flood protection level (or levee height) H(t), (c) the distance of the center of mass of the human settlement from the river D(t), (d) the size of the human settlement G(t), (e) the intensity of flooding events F(t), and (f) the social awareness of the flood risk M(t) simulated by 5000 ensembles with uncertain high water levels and no data assimilation in the experiment 2 (see section

3.1.2). The time step is annual. Grey, red, and black lines are the ensemble members, their mean, and the synthetic truth, respectively.

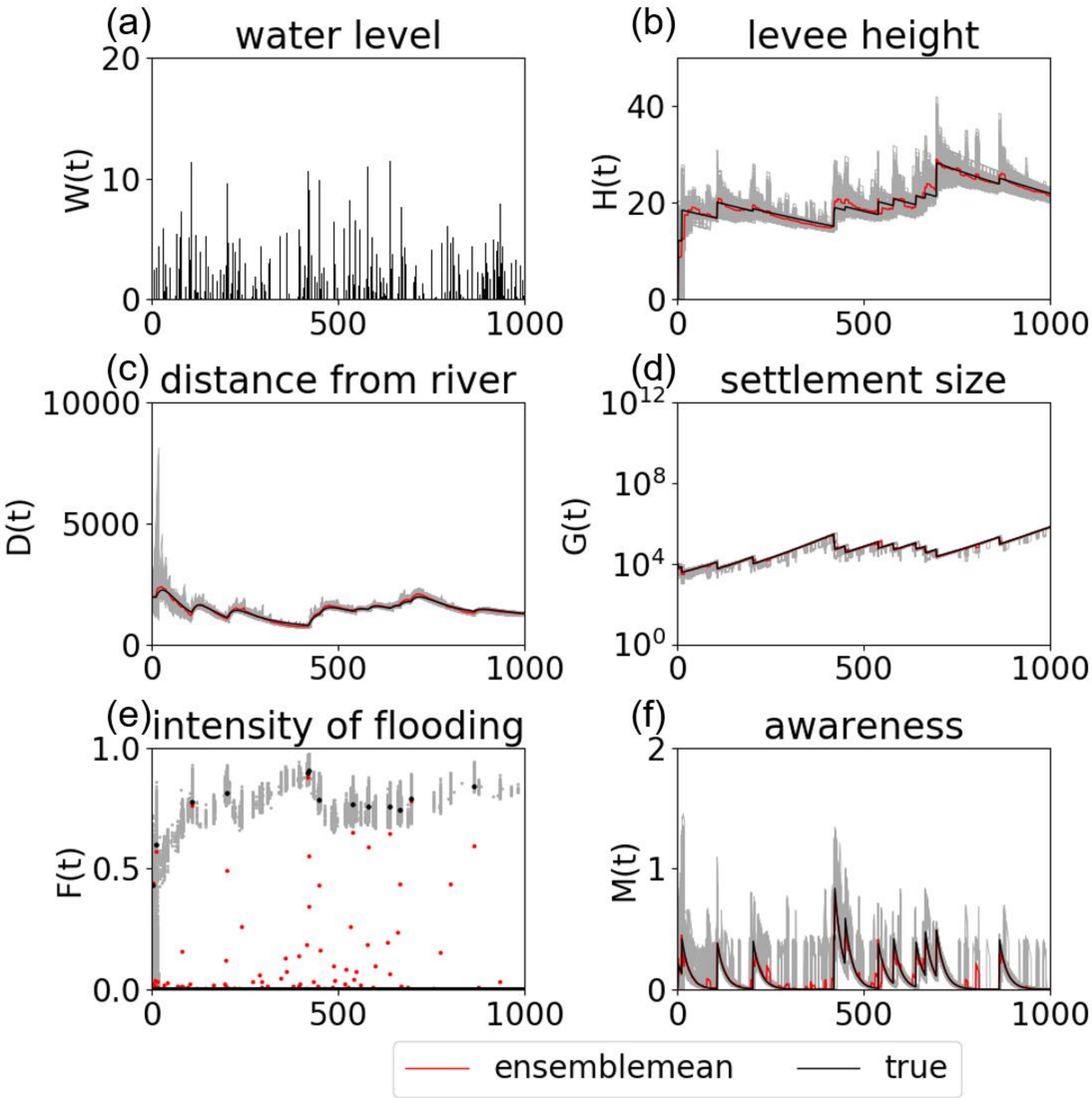

Figure 6. Timeseries of (a) high water level W(t), (b) the flood protection level (or levee height) H(t), (c) the distance of the center of mass of the human settlement from the river D(t), (d) the size of the human settlement G(t), (e) the intensity of flooding events F(t), and (f) the social awareness of the flood risk M(t) simulated by the data assimilation experiment in which the observations of F, G, D, H, and M are assimilated into the model

every 10 years with 5000 ensembles in the experiment 2 (see section 3.1.2). The time step is annual. Grey, red, and black lines are the ensemble members, their mean, and the synthetic truth, respectively.

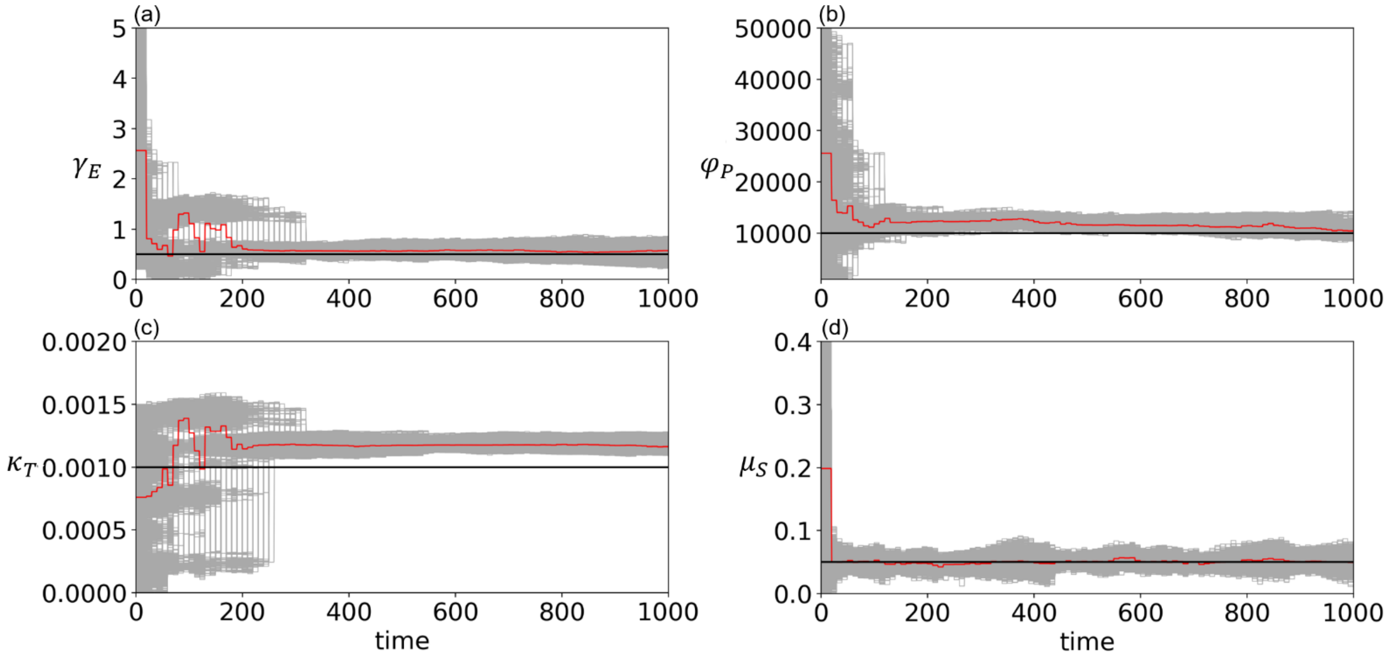

Figure 7. Timeseries of (a) the cost of levee raising γ_E, (b) the rate by which new properties can be built φ_P, (c) the rate of decay of levees κ_T, (d) memory loss rate μ_S estimated by the data assimilation of all observations (F, G, D, H, and M) with 5000 ensembles every 10 years in the experiment 2 (see section 3.1.2). The time step is annual. Grey, red, and black lines are the ensemble members, their mean, and the synthetic truth, respectively.

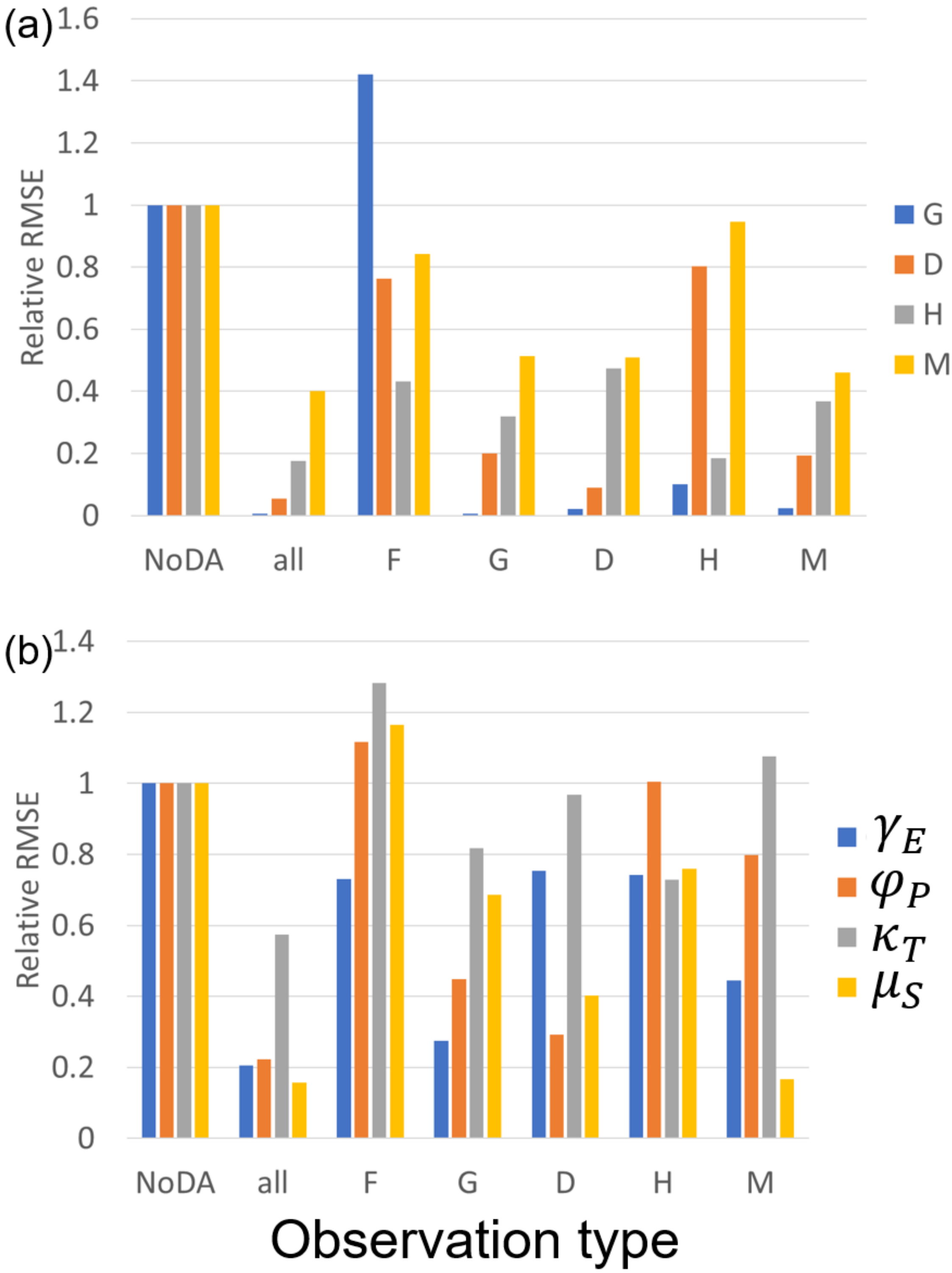

Figure 8. The ratio of RMSEs of the no data assimilation experiment (NoDA) to those of the data assimilation experiments in which all of observations (F, G, D, H, and M) are assimilated (all) and each one of them is assimilated in the experiment 2 (see section 3.1.2). (a) Blue, orange, gray, and yellow bars are RMSEs of the

size of the human settlement G(t), the center of mass of the human settlement from the river D(t), the flood protection level (or levee height) H(t), and the social awareness of the flood risk M(t). (b) Blue, orange, gray, and yellow bars are RMSEs of the cost of levee raising γ_E, the rate by which new properties can be built φ_P, the rate of decay of levees κ_T, memory loss rate μ_S.

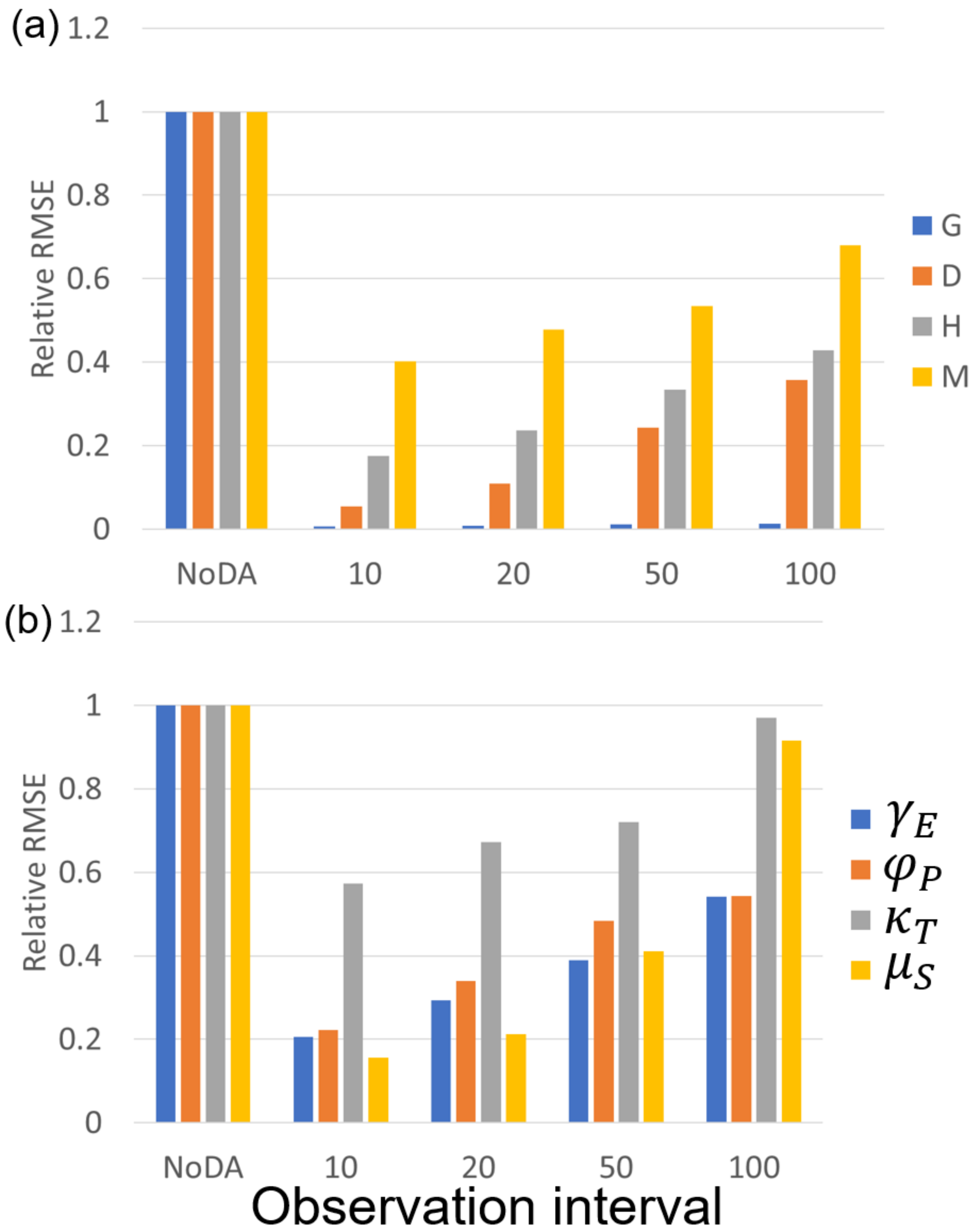

Figure 9. The ratio of RMSEs of the no data assimilation experiment (NoDA) to those of the data assimilation experiments in which all of observations (F, G, D, H, and M) are assimilated every 10, 20, 50, and 100 years in the experiment 2 (see section 3.1.2). (a) Blue, orange, gray, and yellow bars are RMSEs of the size of the

human settlement G(t), the center of mass of the human settlement from the river D(t), the flood protection level (or levee height) H(t), and the social awareness of the flood risk M(t). (b) Blue, orange, gray, and yellow bars are RMSEs of the cost of levee raising γ_E, the rate by which new properties can be built φ_P, the rate of decay of levees κ_T, memory loss rate μ_S.

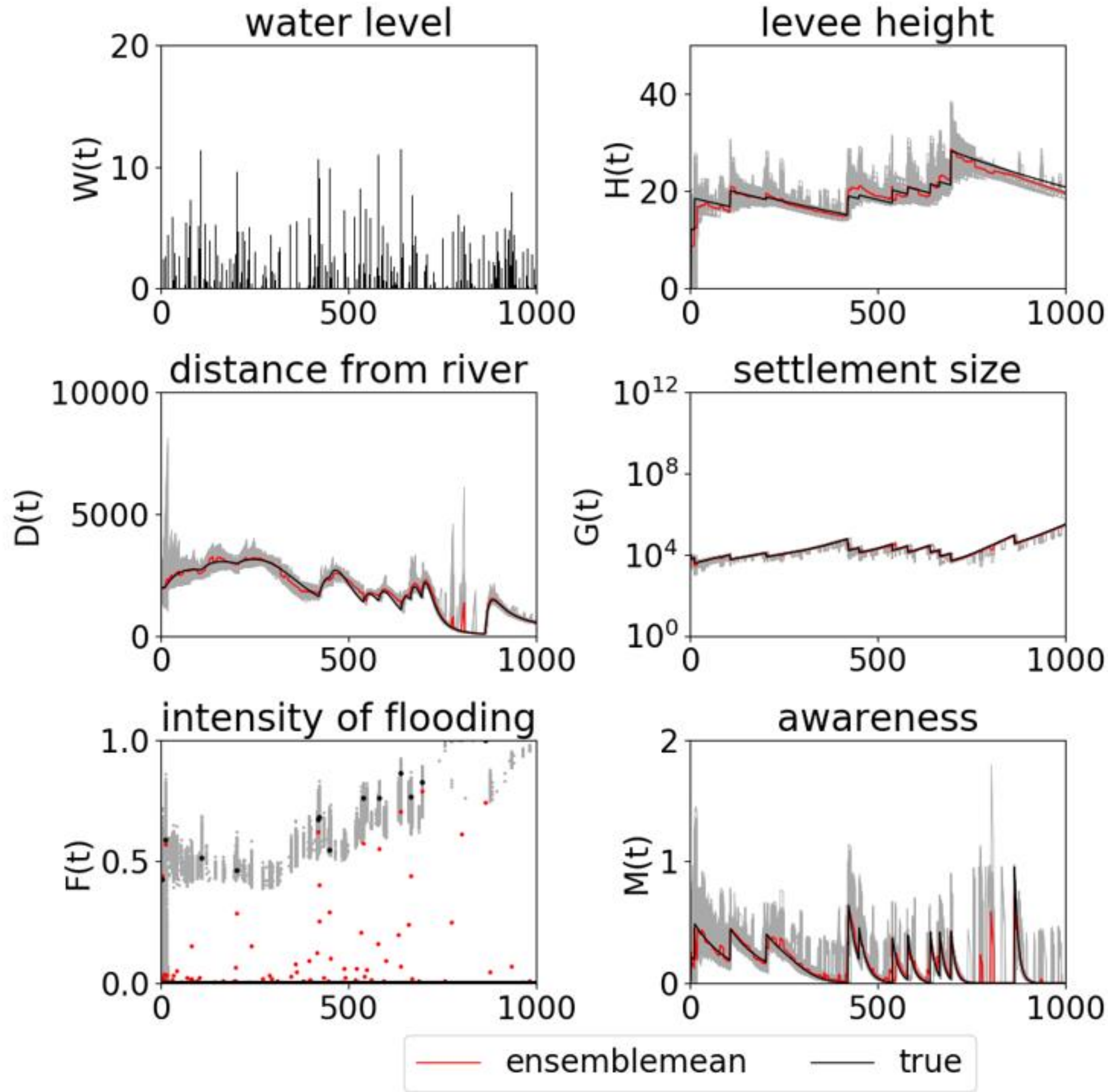

Figure 10. Timeseries of (a) high water level W(t), (b) the flood protection level (or levee height) H(t), (c) the distance of the center of mass of the human settlement from the river D(t), (d) the size of the human settlement G(t), (e) the intensity of flooding events F(t), and (f) the social awareness of the flood risk M(t) simulated by the data assimilation experiment in which the observations of F, G, D, H, and M are assimilated into the model

every 10 years with 5000 ensembles in the experiment 3 (see section 3.1.3). The time step is annual. Grey, red, and black lines are the ensemble members, their mean, and the synthetic truth, respectively.

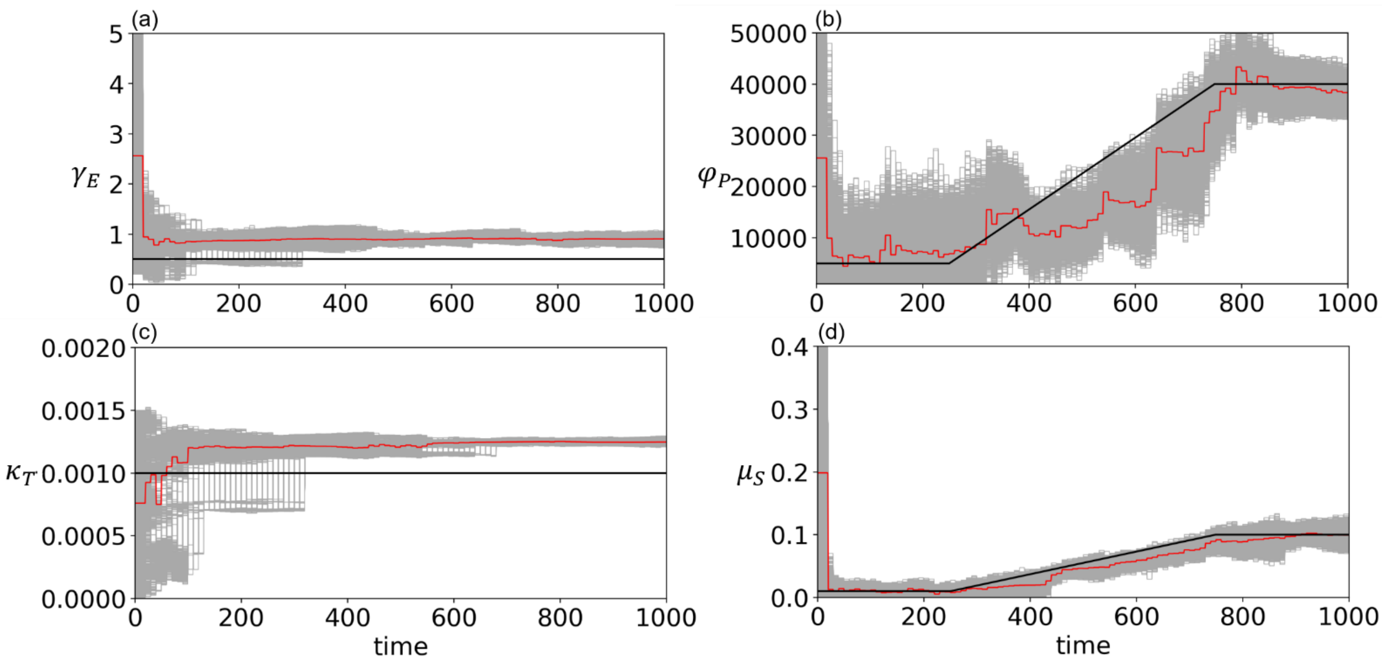

Figure 11. Timeseries of (a) the cost of levee raising γ_E, (b) the rate by which new properties can be built φ_P, (c) the rate of decay of levees κ_T, (d) memory loss rate μ_S estimated by the data assimilation of all observations (F, G, D, H, and M) with 5000 ensembles every 10 years in the experiment 3 (see section 3.1.3). The time step is annual. Grey, red, and black lines are the ensemble members, their mean, and the synthetic truth, respectively.

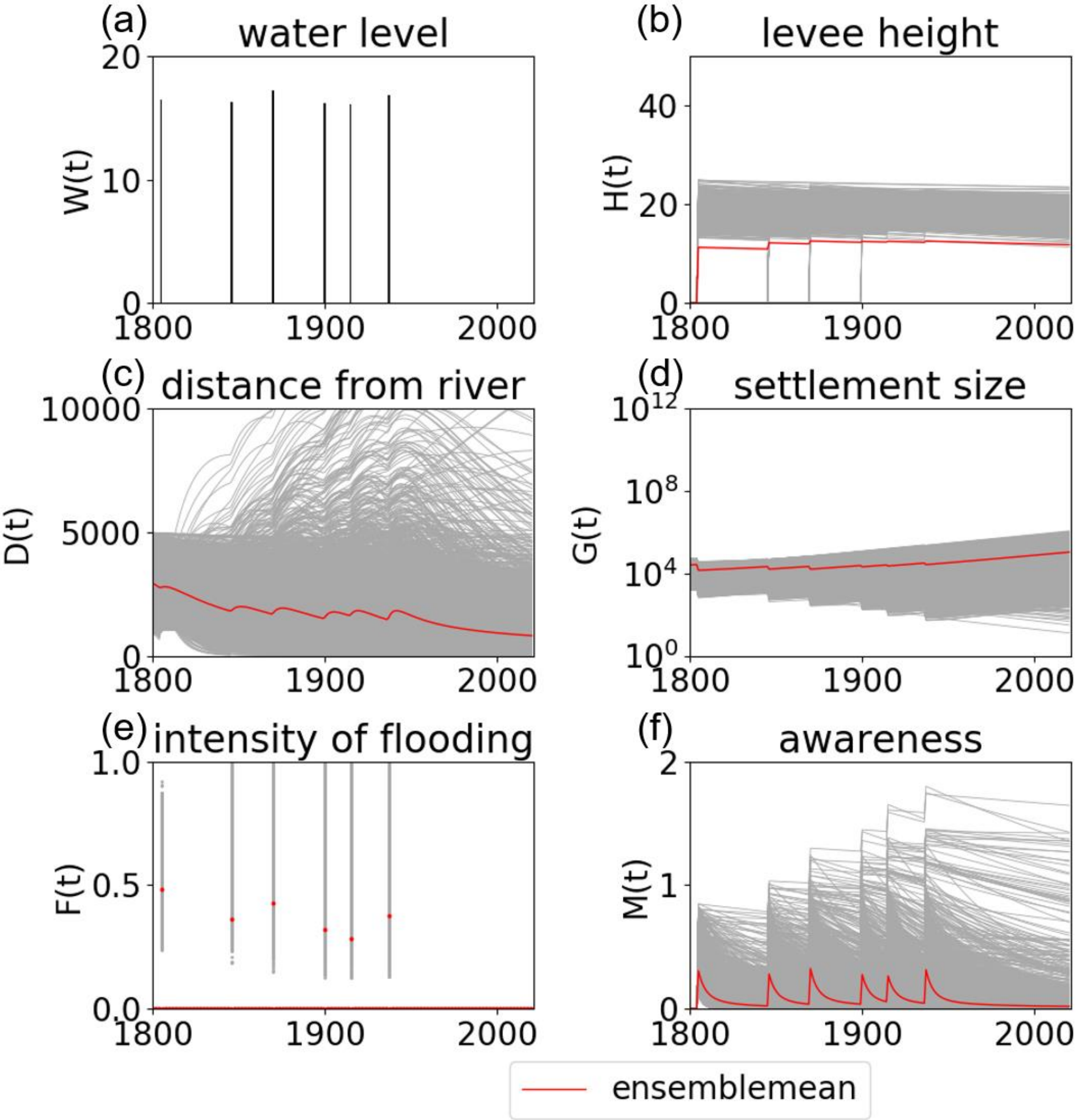

Figure 12. Timeseries of (a) high water level W(t), (b) the flood protection level (or levee height) H(t), (c) the distance of the center of mass of the human settlement from the river D(t), (d) the size of the human settlement G(t), (e) the intensity of flooding events F(t), and (f) the social awareness of the flood risk M(t) simulated by 5000 ensembles with uncertain high water levels and no data assimilation in the real-world experiment in the

city of Rome. The time step is annual. Grey, and red lines are the ensemble members and their mean, respectively.

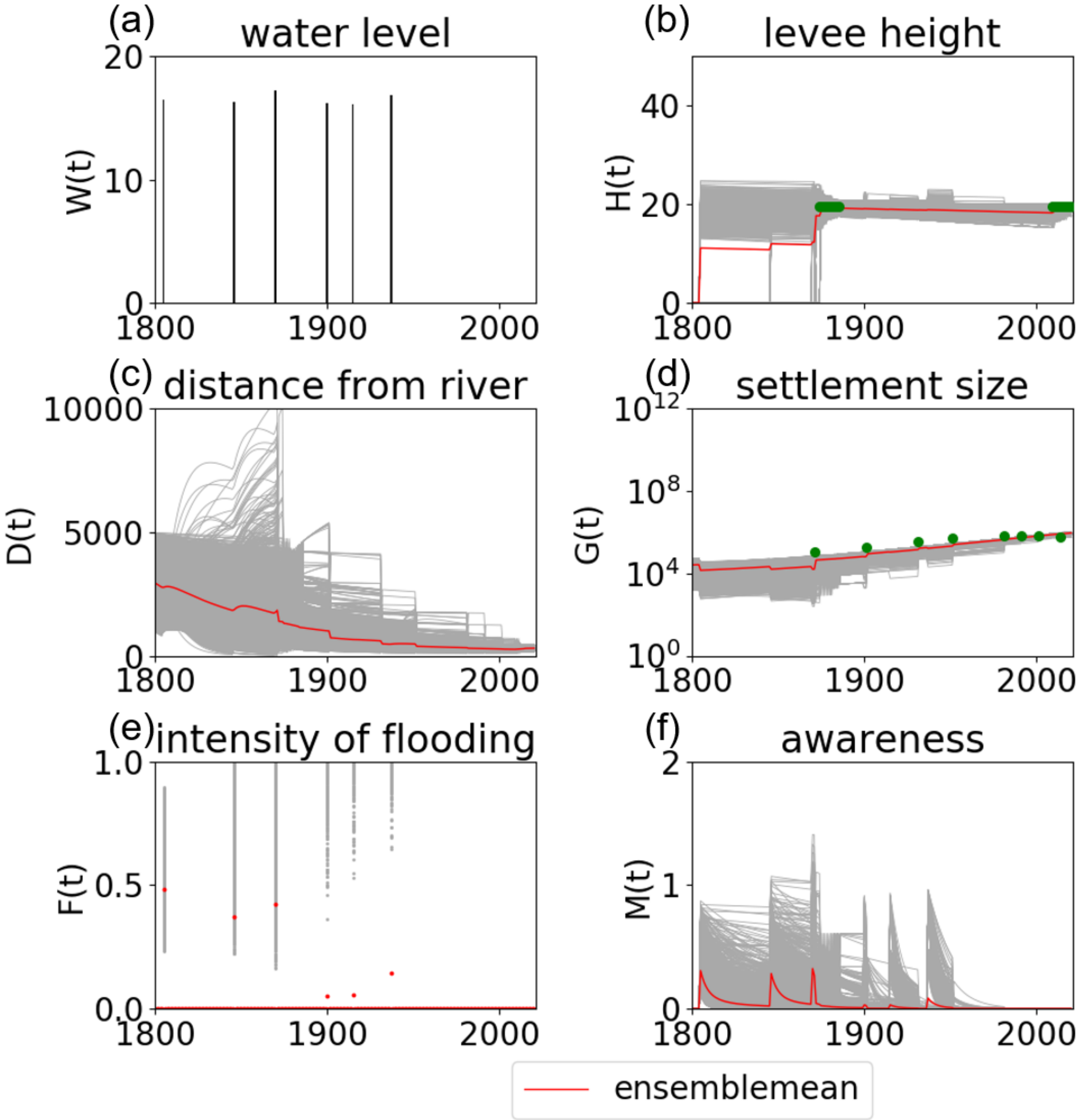

Figure 13. Timeseries of (a) high water level W(t), (b) the flood protection level (or levee height) H(t), (c) the distance of the center of mass of the human settlement from the river D(t), (d) the size of the human settlement G(t), (e) the intensity of flooding events F(t), and (f) the social awareness of the flood risk M(t) simulated by the data assimilation experiment in which the real-world observations of G and H (green dots) are assimilated

into the model with 5000 ensembles in the real-world experiment in the city of Rome. The time step is annual. Grey, and red lines are the ensemble members and their mean, respectively.

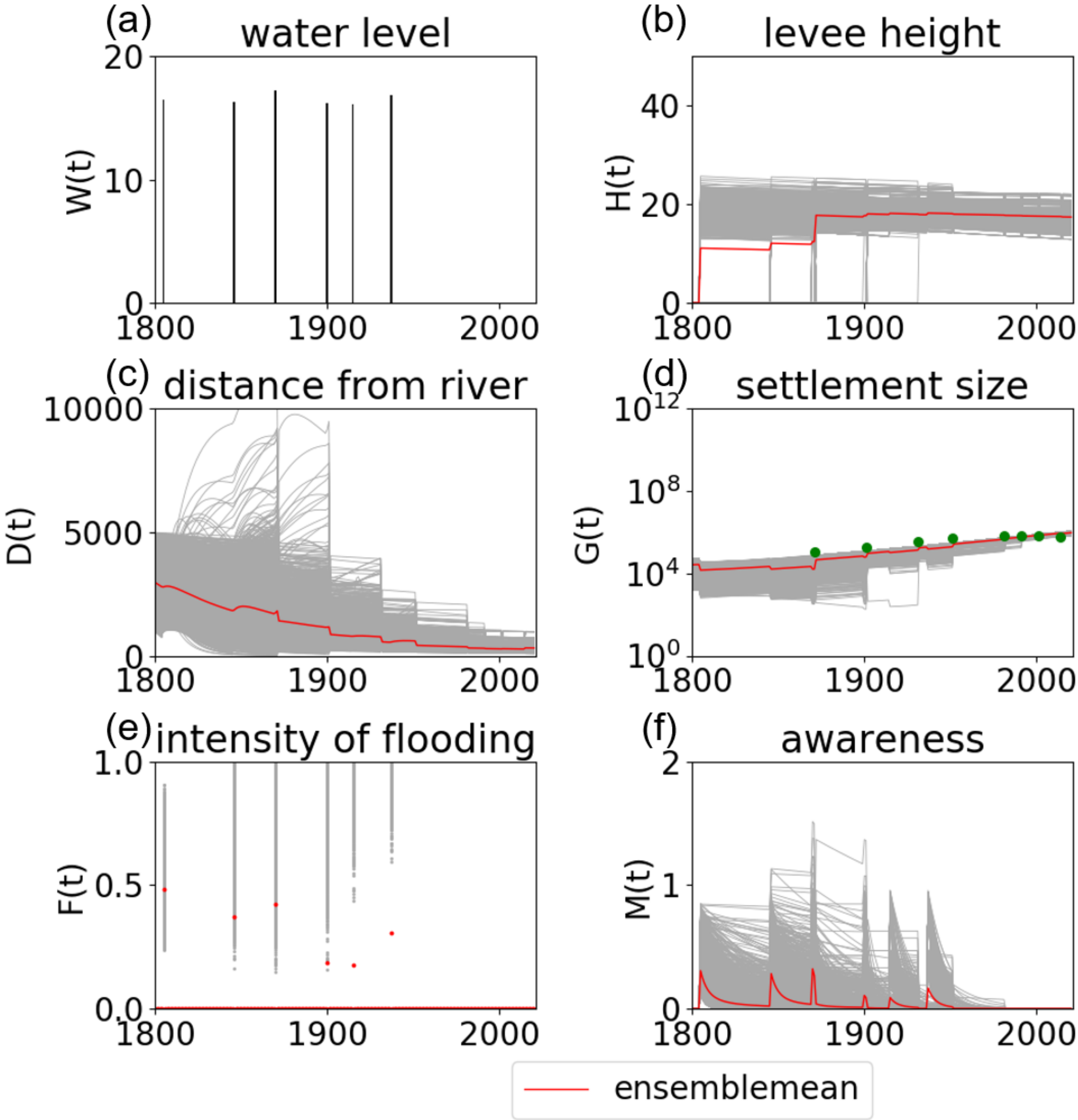

Figure 14. Same as Figure 13 but only real data of G are assimilated.

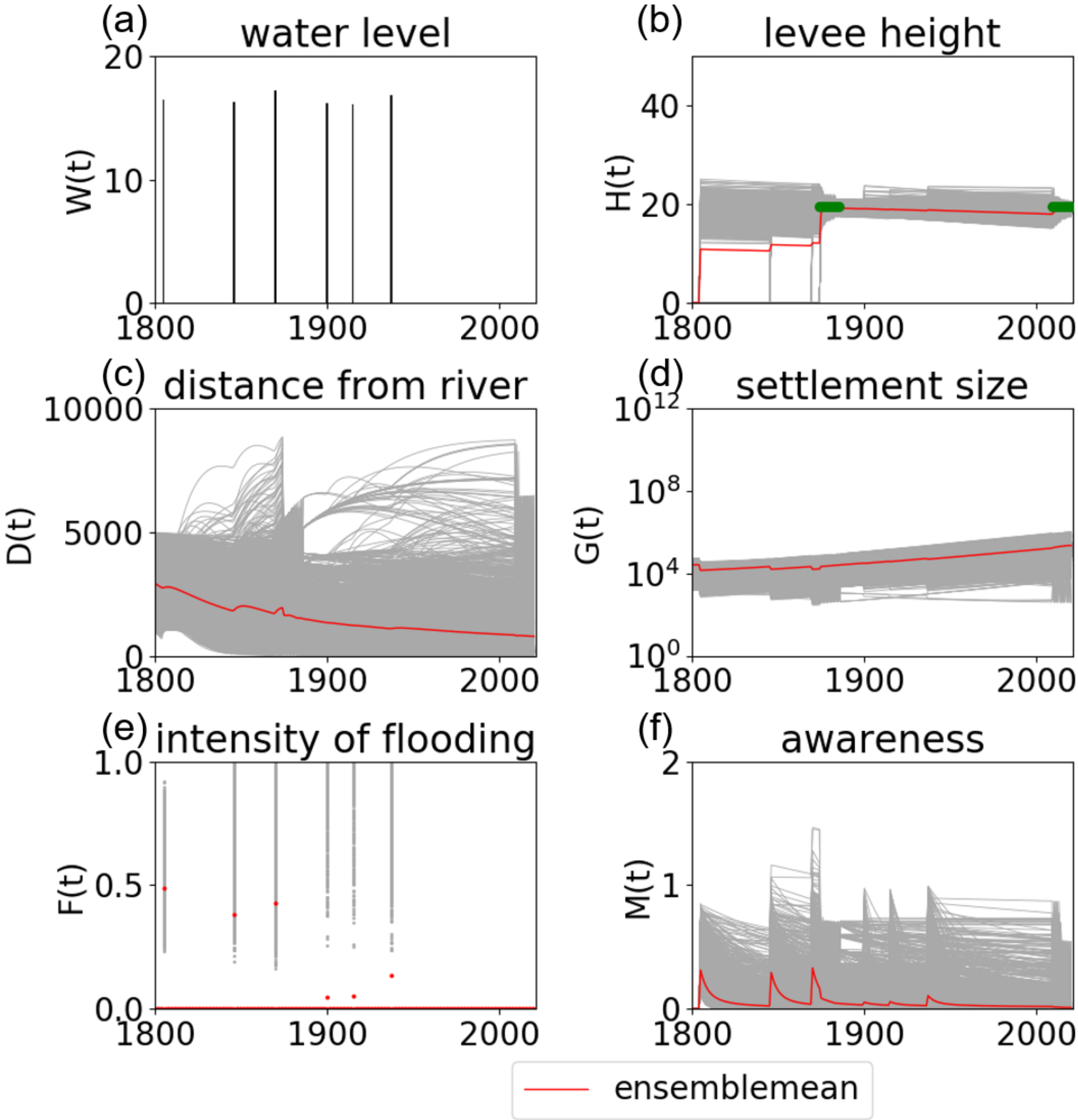

Figure 15. Same as Figure 13 but only real data of H are assimilated.